J. Webster (ed.), *Wiley Encyclopedia of Electrical and Electronics Engineering*

HYDROELECTRIC POWER STATIONS

Water is one of the oldest renewable and clean energy sources, and was one of the first sources used for power generation. When one looks at dam construction and the development of water resources, it is evident that, in the future, hydropower will continue to play an important role in energy production throughout the world.

The type of dam used depends on the geological, geophysical, and topographical conditions existing at the envisaged sites. In recent years, their impact on the environment has also become increasingly important.

The types of dams can be classified as in Table 1. A list of the world's highest embankment dams is given in Table 2.

In 1995, there was 634 GW of hydroelectric capacity worldwide, generating about 2460 TWh/yr, and hydropower now supplies about 18.5% of the world's electricity. In many countries, hydropower provides more than 50% of the national electricity supply, and, in a few of them, more than 90%.

It is clear that there is an increasing trend towards pumped-storage development, that there is a steady increase in capacity due to large-scale schemes in Asia and Latin America, that significant refurbishment and power-plant extensions are under way in Europe and North America, and that there is a healthy level of activity in the field of small hydropower worldwide.

In many of the Asian and Latin American countries, where the greatest potential for future development lies, efforts now being made to accelerate hydropower development by encouraging private investment, and several binational power purchase agreements are giving an added impetus to development plans.

In Asia, China continues to pursue ambitious plans to exploit its vast hydropower resources, with 80 GW being planned in the long term. By the year 2000, the country's installed hydropower capacity will be increased from the present 53 GW to 70 GW. India has 10 GW under construction, and a further 28 GW planned.

In Latin America, Brazil has more than 10 GW of hydropower capacity under construction, and is planning a further 20 GW. Mexico has identified projects totaling nearly 5 GW, of which about 2 GW are planned to be implemented soon.

In Europe, extensive reconstruction projects are under way or being planned in Albania and in Bosnia and Herzegovina. Croatia and Slovenia both have new projects and are planning power-plant extensions. In addition, Greece, Iceland, Macedonia, Spain, and Portugal all have a high degree of hydropower development activity.

In North America, Canada has plans for new schemes and power-plant extensions totaling 10.25 GW in five provinces, of which about one-third are scheduled for implementation by the year 2011.

In Africa, Asia, and the Middle East, there are major dam construction programs under way for water supply, irrigation and hydropower. Notable examples are in Iran, Algeria, Turkey, Korea, Jordan, and China.

Nevertheless, hydropower has had to face some challenging constraints in the past few years, including public opposition on environmental grounds, and increasingly complex regulatory procedures. Furthermore, trends towards private investment, while accelerating development plans, have also led to new complexities in financing and risk management.

Table 1. Dam Classification

Type	Abbreviation
Arch	a
Buttress	b
Earthfill	e
Gravity	g
Multiarch	m
Rockfill	r
Roller-compactedconcrete	rcc

Table 2. World's Highest Embankment Dams

No.	Name	Year of Completion	Country	Type	Height (m)
1	Rogun	1990	USSR	e/r	300
2	Nurek	1980	USSR	e	300
3	Chicoasen	1980	Mexico	e/r	261
4	Tehri	1995	India	e/r	261
5	Kishau	1995	India	e/r	253
6	Guavio	1989	Colombia	e/r	246
7	Mica	1973	Canada	e/r	242
8	Chivor	1975	Colombia	e/r	237
9	Oroville	1968	USA	e	230
10	Upper Mill Branch Tailings	1963	USA	e	213
11	Keban	1974	Turkey	e/g	207

Source: International Commission on Large Dams.

Hydroelectric Layouts

There are three principal types of arrangement for hydroelectric power plants, namely storage, pure pump–turbine, and mixed pump–turbine. They are briefly described below:

(1) Storage Power Plants Only a part of the water is used immediately. The rest is stored in a reservoir for later use. The water can also be provided by additional pumping plants. Run-of-the-river plants in the pre-Alpine regions or upstream of reservoirs, which produce a significant portion of their energy by profiting from the mode of operation of the upstream plants (which they can influence significantly), are also classed as storage power plants if the energy represented by the volume of water stored in the upstream reservoir is greater than or equal to 25% of the mean predicted winter production.

(2) Pure Pump–Turbine Power Plants These only use water that has been previously pumped into the storage reservoir. As a general rule, the pumps and the turbines have the same storage and lower reservoirs. In the

turbine mode, the units are operated with high energy prices during the peak loads, whereas in the pump mode they work at night at a low energy price.

(3) Mixed Pump–Turbine Power Plants These are a combination of a storage power plant and a pure pump–turbine power plant.

For countries whose production of electric energy depends primarily on hydroelectric power plants (for example, Austria, Switzerland), storage power plants play a predominant role. They are used for converting summer energy into winter energy. The energy provided by the melting of snow and of glaciers during the summer is retained behind dams located in the high Alpine valleys, to be utilized during the winter in the storage power plant turbines. Because plants arranged in this way rapidly attain their nominal load (in 60 to 180 s), they are very well adapted to the absorption of peak loads.

In practice, the consumption of energy varies considerably during the day, and shows very pronounced peaks (see Table 3), which can be compensated by the storage power plants. The latter therefore fulfil an important function, particularly in interconnected networks (e.g. in Western Europe), where the majority of the park consists of thermal power plants.

Thanks to their simple regulation system, storage power plants are also used to compensate the small, continuous variations in the network. They also permit the export of peak energy during the colder days of winter, at a profitable price, to compensate for the import of basic energy during periods of low demand, at a considerably lower price.

Basic Criteria for the Design of the Main Equipment of a Hydropower Plant

The choice of the main equipment to be installed in a power plant, such as the inlet valve, turbine, generator, transformer, and screened bus bars, is based on numerous criteria, which have all to be analyzed and studied in order to achieve an optimal plant design. The design study should at least cover the following aspects:

(1) For Turbines and Inlet Valves

- Choice of the turbine outputs for total, rated, minimum, and maximum net heads (P_t, H_n, H_{min}, H_{max})
- Choice of the rated and specific turbine speeds (n_n, n_q)
- Analysis of the expected runaway speed (n_r)
- Cavitation behavior and turbine spiral case setting, choice of σ value, and permissible cavitation damage
- Choice of the operating ranges, such as power, net head, and duration of operation
- Turbine efficiency and choice of the weighting factors
- Hydraulic steady- and transient-state conditions
- Draft tube and spiral case pressure fluctuations and power swings
- Analysis of the main design requirements, such as geometrical dimensions, material quality, definition of deflection, and fatigue limits, for the main turbine components:
  - Spiral case
  - Stay vane
  - Runner
  - Head cover and bottom ring
  - Draft tube
  - Shaft seal

Table 3. Available Capacity and Actual Daily Load of Swiss Network on September 15, 1993

(a) Available Capacity

x Run-of-river hydro power plants (at average daily inflow)	2225 MW = 16.3%
x Hydrostorage power plants (at 95% of installed capacity)	7750 MW = 56.3%
x Nuclear and thermal power plants	3750 MW = 27.4%
Total	P_a = 13585 MW = 100%

(b) Effective Peak Loads

x Peak load of total generation	P_{max} = 10080 MW
x Peak load of the Swiss consumption (included pumped storage consumption)	P_{max} = 7390 MW
x Excess peak load for export	P_{max} = 2690 MW

(c) Daily Load Diagram

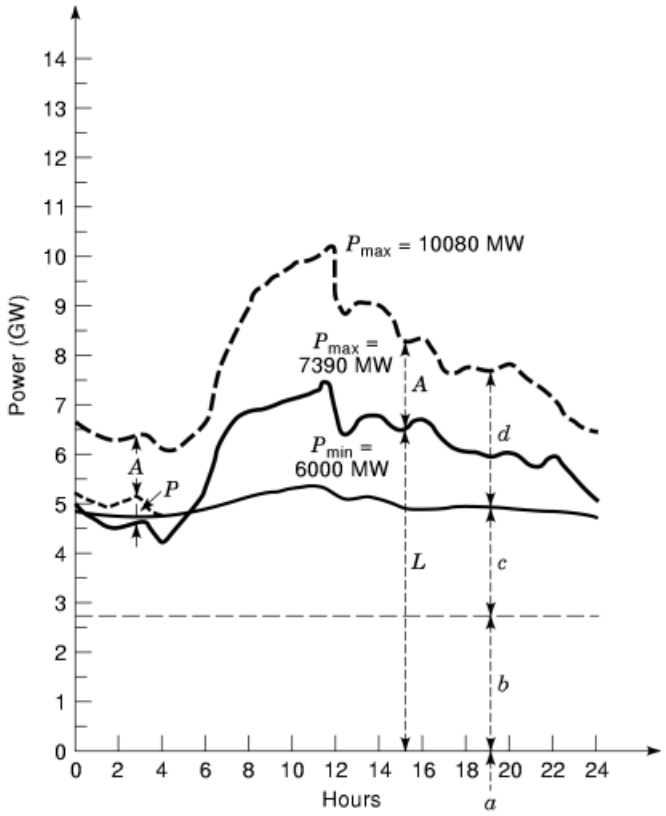

a = generation of conventional thermal power plants
b = generation of nuclear power plants
c = generation of run-of-river hydropower plants
d = generation of hydrostorage power plants
A = excess for export
L = Swiss country consumption (without consumption for hydrostorage power plants)
P = consumption of pumped power plants

(d) Net Energy Generation on September 15, 1993

x Generation of conventional thermal power plants	2.1 GWh = 1.1%
x Generation of nuclear power plants	62.3 GWh = 33.6%
x Generation of run-of-river hydropower plants	53.4 GWh = 28.8%
x Generation of hydrostorage power plants	67.5 GWh = 36.5%
Total net generation	E_d = 185.2 GWh = 100%
x Swiss consumption	E_n = 143.6 GWh = 77.5%
x Export energy	E_{ex} = 41.6 GWh = 22.5%

Table 3. *(Continued)*

Quantities that can be determined from the above daily load diagram:

1. *Daily availability factor* f_a: The ratio between daily net generation E_d (MWh) and available capacity P_a (MW) over 24 h,

$$f_a = \frac{E_d}{24P_a} = \frac{185{,}200}{24 \times 13{,}725} = 0.562$$

2. *Daily load factor* f_L: The ratio between daily net generation E_d (MWh) and peak load P_{max} (MW) over 24 h,

$$f_L = \frac{E_d}{24P_{max}} = \frac{185{,}00}{4 \times 10{,}080} = 0.765$$

3. *Daily duration referred to available capacity* t_a: The ratio between daily net generation E_d (MWh) and available capacity P_a (MW)

$$t_a = \frac{E_d}{P_a} = 24f_a = 13.49\ \text{h}$$

4. *Daily duration referred to peak load* t_L: The ratio between net generation E_d (MWh) and peak load P_{max} (MW),

$$t_L = \frac{E_d}{P_{max}} = 24f_L = 18.37\ \text{h}$$

5. *Ratio between daily minimum load* P_{min} (MW) *and peak load* P_{max} (MW):

$$P = \frac{P_{min}}{P_{max}} = \frac{6000}{10{,}080} = 0.595$$

General relation between f_L and p:

$$p \approx (0.95 \text{ to } 1.05) \times f_L^2$$

6. *Reserve rotation factor* r: The ratio between available capacity P_a (MW) and peak load P_{max} (MW),

$$r = \frac{P_a}{P_{max}} = \frac{13{,}725}{10{,}080} \approx 1.36 \qquad \text{(36\% rotation capacity)}$$

- Guide bearing
- Regulating mechanism
- Governor
- Auxiliary equipment

Model test of the turbine according to authoritative standards; determination of the prototype performance from model acceptance tests, taking scale effects in consideration Analysis of the resonance frequency between penstock, turbine, generator, and network Maximizing the reliability and serviceability of the turbine components Main design of the inlet valve, including rated diameter, design and test heads, rated and maximum discharges, breakdown discharge Transport constraints for turbine and inlet valve components Manufacturing and erection facility for turbine and inlet valve components

(2) For Generatoers

- Choice of rated and maximum apparent power at rated power factor, for over- and underexcited modes
- Choice of rated generator voltage with permissible voltage range
- Analysis of rotor stress at runaway speed
- Choice of the permissible temperature rise for stator and rotor windings
- Choice of the generator utilization factor (Esson coefficient)
- Choice of the moment of inertia in accordance with the turbine regulation conditions
- Choice of the reactances and time constants (synchronous, transient, and subtransient) in the direct and quadrature axes
- Cooling system
- Bearings and shaft arrangements, first critical speed
- Braking system
- Synchronous condenser operation, if any
- Excitation system, cooling, voltage, exciter response
- Behavior of the generator–turbine set: vibration and noise levels, choice of the monitoring equipment for the air gap, partial discharge, vibrations, and so on
- Transport constraints for generator components
- Manufacturing and erection facility for generator components

Design Criteria for the Power Transformer. The type of construction chosen for the design of a power transformer depends on many factors, which are principally:

- Possible transportation difficulties from the manufacturing factory to the installation site
- Installation of the transformers in caverns or in the open
- Short-circuit power of the high-tension (*HT*) network (over the long term)
- Maximum voltage limits of the HT network
- Whether it is possible to handle the complete range of these voltage variations by means of a regulator on the generator

For reasons of cost, a three-phase unit is generally favored in caverns. These units are cheaper than single-phase transformers for the same power, and, above all, their installation in caverns requires less space, which is also an advantage to the civil engineer. The realization costs of a triangular unit with armored bars, for a single-phase design, is rather costly and requires a great deal of space.

On the other hand, by choosing a single-phase transformer, the transport difficulties are considerably reduced, and, in order to ensure the maximum availability of the supply of energy, it is sufficient to have one single-phase unit available in reserve.

Although initially more expensive, the series arrangement may prove to be more advantageous for an open-air installation, depending on the number of transformers necessary for the realization of the installation.

The next question that will face the designer is whether the voltage regulation should be provided by the transformer or by the generator. If the calculation of the regulation range necessary to be able to satisfy all the application conditions does not exceed 10% of the generator voltage, it would be advantageous to prefer voltage regulation by the generator. This solution avoids changing the taps on the transformer and thus makes the power transformers more reliable, while providing smooth voltage regulation.

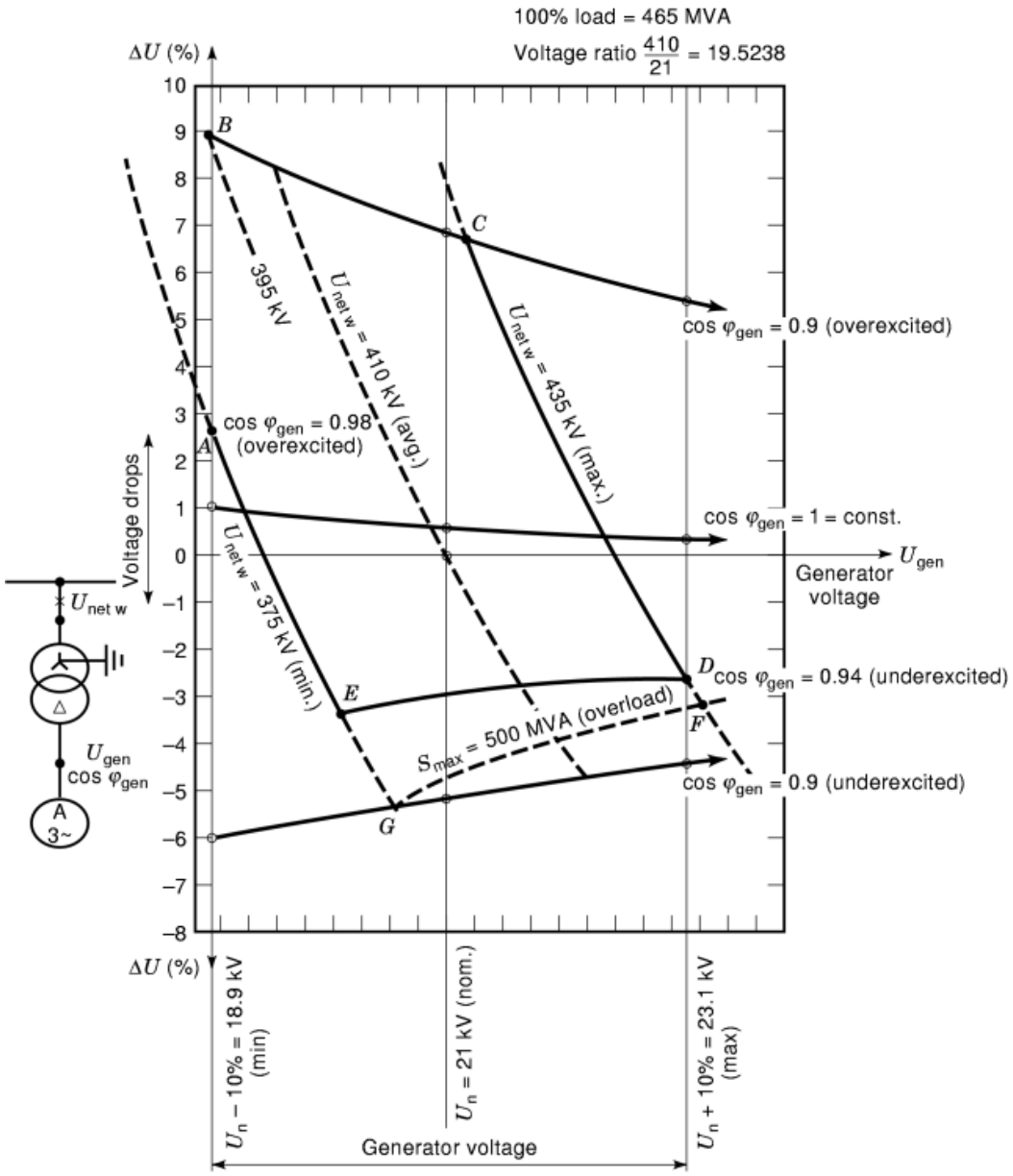

Fig. 1. Voltage drops of the step-up transformer for Bieudron power plant, Switzerland, as a function of the load–generator voltage, under a given rating of 465 MVA.

Figure 1 shows an example of the transformation ratio calculation to be chosen in order to satisfy all the demands of the high-voltage network. In this example, the maximum voltage limits are 375 kV and 435 kV respectively. The table in the legend shows the guaranteed functional range for various generator power factors within the inductive and capacitive limits of the HT network. In any case, where these parts are supplied by different companies, the layout designer must bring about a close collaboration between the transformer

and generator designers, since it is usually impossible to obtain the ideal characteristics of each element. A compromise will have to be found, because two of the constraints are diametrically opposed, namely:

- For the *transformer,* a rather high short-circuit voltage is needed, in order to reduce as far as possible the constraints due to the short-circuit loading, which verge on 60 kA for a standard 400 kV network.
- For the *generator,* the stability of the generator demands a short-circuit voltage that is as low as possible.

Although the power transformers are simplified by the absence of tap changers, their service life nevertheless remains directly linked to their operating temperature. It is clear that the measurement of this parameter is essential in order to be able to estimate the amount of service life remaining, or for a rapid diagnosis of an abnormal temperature rise caused by the poor functioning of the cooling system, or for other reasons. The rapid detection of such faults is an essential condition for avoiding a pronounced degradation of the insulation system.

Point	Network Voltage (kV)	Gen. Voltage U (kV)	Power Factor	Transf. Voltage Drop (%)
A	375 (minimum)	18.9	0.98 (overexcited)	P2.8
B	395 (intermed.)	18.9	0.9 (overexcited)	P8.9
C	435 (maximum)	P21.2	0.9 (overexcited)	P6.8
D	435 (maximum)	23.1	0.94 (underexcited)	P2.5
E	375 (minimum)	P20	0.94 (underexcited)	P3.3

The classical measurement systems do not allow the conductor temperature to be determined. Systems using fiber optics for point measurement are available on the market. Their use, however requires prior knowledge of the positions that are most exposed thermally. In addition, this technique only allows monitoring of a single, well-defined zone of the machine.

The use of the new technology of fiber-optic distributed sensors provides a temperature profile, which can allow this disadvantage to be avoided (see Fig. 2). Contrary to the conventional point technique, in which the temperature measurement is carried out by means of a sensor specially positioned at the extremity of the fiber, the new distributed temperature sensor (DTS) technology is based on a totally different principle. The measurement is effectively carried out along the length of the fiber (diameter 0.15 mm to 0.6 mm), thereby allowing the acquisition of an much larger amount of information, while maintaining sufficient precision ($\pm$ 2°C, $\pm$ 1 m).

A short-duration light impulse, produced by a laser, is sent at a high rate into a multimode optical fiber. The physical properties of the reflected light signal are modified by the temperature. In order to improve the sensitivity of the system, one must provide means for eliminating the background noise.

The principle adopted is measurement by means of optical reflectometry with a slow operating range, which measures the Raman backscatter over the complete length of the fiber. When a laser impulse is sent through the fiber, the incident light is attenuated in all directions by absorption and diffusion. Some of the light is dispersed at frequencies different from that of the incident light. The spectrum of the dispersed light is dominated by Rayleigh dispersion, but the phenomenon of Raman dispersion also occurs with a lower incidence, and its anti-Stokes component is sensitive to temperature.

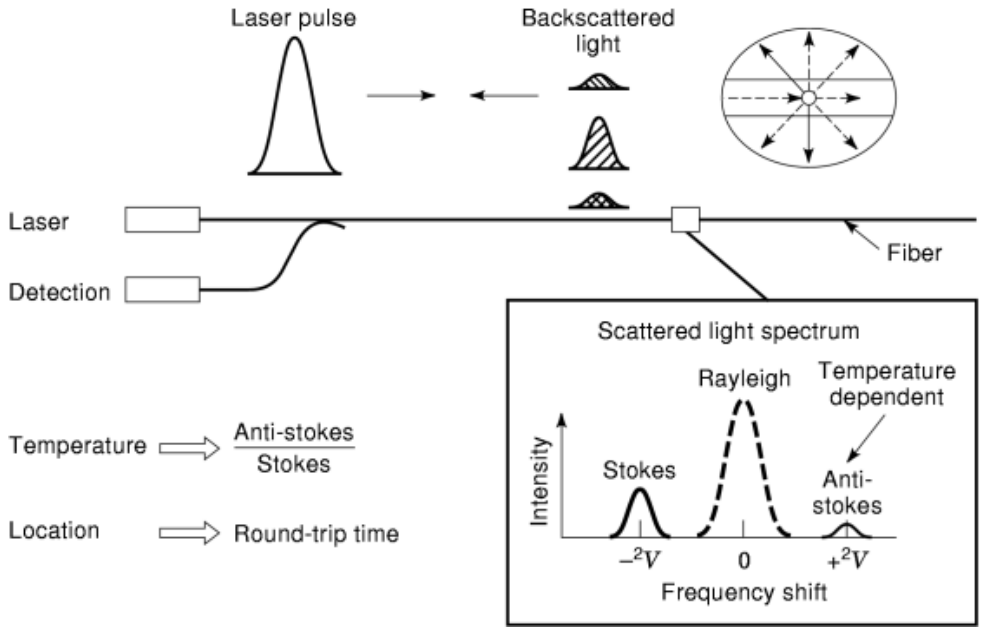

Fig. 2. Distributed temperature sensor.

The location of all the various changes in the backscattered light may be calculated by measuring the elapsed time during the last impulse (incident journey plus return journey). Using this technique, it is possible to effect about three measuring points per turn on the winding of a power transformer.

In the case of a three-phase 500 MVA transformer, given a voltage ratio of 20/400 kV, the circumference of one turn of the low-tension winding exceeds 4 m. With a fiber-optic resolution of 1 m, this gives more than four measuring points per turn. Given that a winding of this kind consists of around 50 turns, it can be seen that there are about 200 measuring points per phase that can be analyzed. This allows one to exactly monitor the temperature behavior of the winding in real time. It is clear that one can proceed in a manner identical to that for magnetic circuits. The multimode fiber is placed directly on the copper by the copper supplier, the winding being carried out in an absolutely conventional manner by the transformer manufacturer.

As the present trend is to look for a maximum availability of the energy production system, the user must rely on predictive methods in order to quickly determine the start of degradation of his material. The aim is to program interventions that, on the one hand, should take place during nonproduction periods, and, on the other, should be able to partially relieve those parts that are beginning to show anomalies.

For this purpose, one can combine a temperature measuring system with a continuous dissolved-gas analysis. These operations are carried out by a unit mounted onto the transformer. The extraction is carried out with the help of a semipermeable fluorosilicone membrane, and the detection by means of hydrogen and other combustible-gas sensors. Together with the physicochemical analysis of the oil and the continuous measurement of its humidity, the set of these predictive measurements will detect 80% of faults or serious incidents sufficiently early to avoid unexpected interruptions of the production of energy.

The improvement of the sheets used for the manufacture of the magnetic circuit of the transformer, as well as the technique of interlining these circuits, has been a spectacular technological development of recent years. Modern iron–silicon magnetic sheets have a structure (steel with oriented grains) that gives them exceptional magnetic properties when the flux is parallel to the direction of the laminations, which is the direction of the easiest magnetization. The improvement in performance has been continual, and at the moment the residual

disorientation of the average grains of a good quality steel (HIB steel) is of the order of 3° to 4°. Modern technology has also been applied to reduce the thickness of these sheets. Irradiation of the surface with a laser beam and the addition of silicon (about 3.2%) also strongly improve the quality of these sheets by notably diminishing the losses due to eddy currents, which reach a minimum for a disorientation of around 2°. With this kind of sheet, the induction can reach 1.95 T for a magnetic field intensity of 800 A/m.

The reduction of hysteresis losses is obtained by the purification of the material, notably by elimination of the carbon through the action of hydrogen at high temperature, and by the addition of silicon depending on the resistance of the sheet, which must be kept sufficiently high to reduce the losses due to eddy currents.

The total energy losses for one cycle of a magnetic sheet may be divided into three components:

(1) The Hysteresis Losses These are a function of the induction B and are proportional to B^n, where n is approximately 2.

(2) The Classical Losses Due to eddy currents, these are expressed by the relation:

$$P_c = \frac{kB_m^2 f^2 eL}{\rho} \qquad \text{(kW)}$$

where

e = thickness of the steel
L = average size of the magnetic domains
B_m = maximal value of the induction inside the material
f = frequency of the applied sinusoidal magnetic field
ρ = resistivity of the Fe–Si alloy

(3) The Abnormal Losses The classical losses due to eddy currents presuppose a uniform sinusoidal movement of the domains at 180°, presumed plane and regularly spaced (L) at the magnetic frequency. The deviation of the relationship from this ideal situation leads to the abnormal losses (P_a) due to eddy currents, which become important at inductions larger than 1 T. The complexity of the structure of the magnetic domains and that of the movement of the walls are the two principal causes of abnormal losses in the magnetic sheets.

Another approach for the reduction of the iron losses of a transformer has been made possible by the appearance on the market of amorphous sheets. This material does not have a crystalline structure, but acts like a glass. The specific losses of these sheets are about 5 times lower than those of conventional sheets. Nevertheless, it must not be forgotten that losses measured in a magnetic circuit are considerably higher than those in the sheets measured separately. The gain in performance is not so obvious if one takes into account the difficulties in handling the material and the fact that magnetic sheets with oriented grains have not yet reached the limits of their potential quality.

Design Criteria for the Generator. Studies of the stability of generators imply that, when making the choice, great attention should be paid to the values of the direct-axis synchronous reactance x_d, the direct-axis transient reactance x'_d, the moment of inertia J, and the acceleration time τ_J.

The acceleration time is the time necessary for accelerating the synchronous machine from rest to the nominal speed, by applying a constant acceleration moment equal to the quotient of the nominal effective power and the nominal angular velocity. This is expressed by the equation

$$\tau_J = \frac{Jw_n^2}{P_n} \qquad \text{(s)}$$

where

τ_J = acceleration time (s)
J = moment of inertia ($t \cdot m^2$)
$w = \pi n_n/30$ = nominal angular velocity (s^{-1})
n_n = rated speed (rpm)
P_n = rated active power (kW)

Studying the influence of the direct-axis synchronous reactance is equivalent to studying that of the short-circuit ratio K_c, which is by definition the ratio of the excitation current that produces the nominal no-load voltage to the excitation current that produces the nominal current in a three-phase short circuit:

$$K_c = \frac{i_{f0}}{i_{fk}}$$

CIGRE recommends the adoption of a short-circuit ratio K_c between 0.65 and 0.9 for a number of poles $2p = 8$ to 14. The synchronous reactance is defined as

$$x_d = \frac{1.08 \text{ to } 1.12}{K_c} \qquad \text{(p.u.)}$$

The direct-axis synchronous reactance x_d may be considered, in practical calculations, as the sum of the values of the leakage reactance x_a of the stator and of the direct-axis reactance x_{ad} of the armature, namely $x_d = x_a + x_{ad}$. But, in this sum, the contribution of x_a is only of the order of 12% to 15% of the total, and it follows that, in order to reduce x_d, one must above all reduce the value of x_{ad}.

The latter is written as

$$x_{ad} = k_d \cdot \frac{\tau_p}{\delta'} \cdot \frac{A_1}{B_{\delta 1}} \qquad \text{(p.u.)}$$

where τ_p is the pole pitch of the machine, δ' the equivalent air gap, and $B_{\delta 1}$ the induction in the air gap. If τ_p is chosen lower, one is led to appreciably reduce the value of the moment of inertia J, which is not desirable. If, on the other hand, one chooses a ratio $A_1/B_{\delta 1}$ that is lower, one ends up with poor electrical utilization of the machine due to the increase of $B_{\delta 1}$. For that reason, the only effective measure consists in increasing the equivalent air gap, $\delta' = K_c\delta$; but this is at the cost of increasing the excitation losses.

It also appears that the choice of x_d is itself a complex problem, in which one must consider, among others, its influence on the price of the machine, the losses, the moment of inertia, and the problems of static stability.

The direct-axis transient reactance x'_d determines the dynamic stability of a synchronous machine. The lower the value of x'_d, the higher the dynamic stability:

$$P_{dyn} = \frac{e'u}{x'_d} \sin\vartheta + \frac{u^2}{2}\left(\frac{1}{x'_q} - \frac{1}{x'_d}\right)\sin 2\vartheta$$

where

P_{dyn} = ratio of the power limited by the dynamic stability to the rated active power (p.u.)
e' = internal transient voltage (behind the transient reactance)
u = voltage at the terminals of the synchronous machine
ϑ = load angle

x'_q = quadrature axis transient reactance (in general $x'_q \approx x_q$)

The value of x'_d is approximately given by the relationship

$$x'_d \approx x_a + \frac{1}{(1/x_{ad}) + (1/x_{fd})} \qquad \text{(p.u.)}$$

in which

x_a = leakage reactance of the stator (p.u.)
x_{ad} = direct-axis armature reaction (p.u.)
x_{fd} = leakage reactance of the rotor (p.u.)

The above relation shows that it is the values of x_a and of x_{fd} that most influence x'_d, because $x_{ad} \geq x_a, x_{fd}$.

A decrease of x'_d by means of x_a is not advisable, because it follows that the subtransient reactance x''_d also decreases, which results in an increase of mechanical stress in the stator windings in the event of a short circuit. For this reason, the only effective means consists in reducing x_{fd} by means of a construction appropriate to the rotor (lower polar plates and larger interpolar spaces), or by the choice of an appropriate ratio $A_1/B_{\delta 1}$. In reducing x'_d, one also reduces the Potier reactance [$x_p = (0.75 \text{ to } 0.85) \times x'_d$], which results in lower excitation losses. These considerations clearly show that one must prescribe the lowest possible value of the direct-axis transient reactance.

According to the CIGRE recommendation, $x'_d = 0.28$ to 0.32 p.u. for classical cooled generators with $2p = 8$ to 14; the influence of the value of the direct-axis transient reactance on the price of a classical cooled machine is practically negligible in the range $x'_d = 0.26$ p.u. to 0.30 p.u. On the other hand, one notes that one must not move in the direction of a very large reduction: for example, for $x'_d = 0.2$ p.u., the price of the machine will not be increased by more than 1%, but, in return, the losses are larger by around 10%, which is highly undesirable.

For generators driven by Pelton turbines and started up many times a day, it is very desirable to invest in electric braking. In fact, these machines are braked during a normal stop, but only by the losses from the ventilation and friction. A group with a power of the order of 500 MVA has such an inertia that the normal stop requires more than 100 min, whereas, with electrical braking by means of short circuit and reexcitation, in general at $1.2I_n$, this time is reduced to around 7 min.

This electric braking system is reliable and has none of the disadvantages of the installation. Moreover, for generators with integral water cooling, electric short-circuit braking does not impose any additional thermal constraints on the stator winding.

As the moment decreases with increasing speed, this brake is not effective in runaway, but is very effective at low speed, so that there is no need for mechanical braking.

The design of the generators, or generator–motors, is determined by the following parameters:

- Rated apparent power S_n (kVA)
- Rated and runaway speeds n_n and n_r (rpm)
- Moment of inertia J ($t \cdot m^2$)
- Synchronous, transient, and subtransient reactances x_d, x'_d, x''_d (p.u.)
- Permissible temperature rises for stator and field windings

The rated apparent power S_n depends on

- The turbine output P_t (kW)
- The turbine efficiency η_t

- The rated power factor cos ϕ

and is given by the following formula:

$$S_n = \frac{\eta_t P_t}{\cos \varphi} \approx \frac{0.94}{0.85} P_t = 1.1 P_t \qquad \text{(kVA)}$$

S_n can also be calculated from the main geometrical and electromagnetic characteristics of the generator:

$$S_n = k \times 1.11 D^2 L n_n A_1 B_{\delta 1} \times 10^{-4} \qquad \text{(kVA)}$$

where

k = wave factor
D = stator bore diameter (m)
L = stator stacking height (m)
n_n = rated speed (rpm)
A_1 = electric loading armature conductor current per unit length (kA/m)
$B_{\delta 1}$ = magnetic loading, average flux per unit area of the air-gap surface (T)

According to CIGRE recommendations, the above figures should be selected within the following ranges for hydrogenerators:

$$k = 1.05 \text{ to } 1.10$$

$$A_1 = \frac{6 I_n N}{\pi D}$$

$$= \begin{cases} 50 \text{ kA/m to } 90 \text{ kA/m}) & \text{for air-cooled generators} \\ 100 \text{ kA/m to } 120 \text{ kA/m} & \text{for water-cooled generators} \end{cases}$$

$$B_{\delta 1} = 0.95 \text{ T to } 1.05 \text{ T}, \qquad \text{independent of the cooling mode}$$

The rotor peripheral velocity v is limited by the construction mode selected. For a laminated rotor rim, v_{max} = 140 m/s to 150 m/s; for massive rotor rim, v_{max} = 200 m/s to 220 m/s. Since v_{max} is given by

$$v_{max} = \frac{\pi D_r n_r}{60} \qquad \text{(m/s)}$$

and

$$D_r = D - 2\delta \qquad \text{(m)}$$

with

D_r = rotor diameter (m)
δ = air gap (m)

it follows that the rotor diameter should not exceed

$$D_r = v_{max} \cdot \frac{60}{\pi n_r} \qquad \text{(m)}$$

The moment of inertia J is a function of the geometrical characteristics of the rotor:

$$J = kD_r^4 L \qquad (\mathrm{t \cdot m^2})$$

A natural moment of inertia J_n is also used, expressed as

$$J_n = \frac{S'_n}{220} \times 2p(2p-3) \qquad (\mathrm{t \cdot m^2})$$

Finally, a very useful figure has been defined that characterizes the design of the generators very well, and allows a rapid comparison of their performance, called the utilization coefficient, or Esson coefficient,

$$C = \frac{S_n}{D^2 L n_n} \approx 0.115 A B_{\delta 1} \qquad (\mathrm{kVA/m^3 \cdot rpm})$$

The Esson coefficient normally takes the following values:

$$C = \begin{cases} 5 \text{ to } 9 & \text{for air-cooled generators} \\ 10 \text{ to } 13 & \text{for water-cooled generators} \end{cases}$$

The results of a design calculation are shown below in an abbreviated form. The generator, from the Bieudron power plant in Switzerland, is fully water-cooled, and is driven by a Pelton turbine:

$$\begin{aligned} S_n &= 465\,\mathrm{MVA} \\ A_1 &= 105.9\,\mathrm{kA/m} \\ B_{\delta 1} &= 1.064\,\mathrm{T} \\ D &= 5.35\,\mathrm{m} \\ L &= 2.9\,\mathrm{m} \\ n_n &= 428.57\,\mathrm{rpm} \\ 2p &= 14 \\ k &= 1.16 \\ C &= 13.07\,\mathrm{kVA/(m^3 \cdot rpm)} \\ J_n &= 1510\,\mathrm{t \cdot m^2} \end{aligned}$$

The layout of the Bieudron power plant is shown in Fig. 3, and the generator operation ranges and load diagram in association with its step-up transformer are shown in Figs. 1, 4, and 5. The power-plant single-line diagram with the excitation, protection, and measurements is shown in Fig. 6, and the corresponding explanatory details in Fig. 7. The auxiliary power supplies from the 380 kV level down to 400 and 230 V ac and 110 V dc can be found in Fig. 8. The main electrical and geometrical characteristics of the generator are given in Table 5.

A diagram of the generator output versus speed, with consideration of the cooling mode and economical limit, is presented in Figure 12. Two of the world's most powerful units with regard to their cooling mode, the Itaipu and Bieudron generators, are shown in this diagram.

Table 4. Main Generator Characteristics of the Bieudron Units[a]

Number of Units	3
Rated frequency f	50 Hz
Rated apparent output S_n	465 MVA
Maximum continuous apparent output S_{max}	500 MVA
Rated voltage U_n	21 kV ± 10%
Rated current I_n	12784 A ± 10%
Rated power factor cos φ	0.9 (0.84)
Rated speed n_n	428.57 rpm
Runaway speed n_r	800 rpm
Number of poles, $2p$	14
Moment of inertia J	$\geq$ 1500 t · m^2
Rated efficiency at cos φ = 0.9 (overexcited)	98.85%
x_{dIn}	≤1.15 p.u.
x'_{dIn}	≤0.35 p.u.
x''_{dUn}	≥0.23 p.u.
Utilization coefficient[b] at rated output, C	13.07 kVA/m^3 · rpm
Cooling system hot-spot temperatures:	
Stator winding (cooled with demineralized water)	67°C
Field winding (cooled with demineralized water)	65°C
Stator core (cooled with row water)	110°C
Stator bore diameter D	5350 mm
Stator stacking height L	2900 mm
Diameter over stator frame, D_e	7700 mm
Pit diameter D_p	10900 mm
Total generator height H	7720 mm
Rotor mass G_r	454 t
Stator mass G_s	290 t
Generator mass G_{TOT}	800 t
Turbine rotor mass G_{RT}	28 t
Thrust bearing load F_{TL}	5250 kN
Specific mass at rated output	1.72 kVA
Specific rated output per pole	33.21 MVA

[a] Fully water-cooled generators, Pelton turbines.
[b] Esson coefficient $C = S_n/D^2Ln_n$.

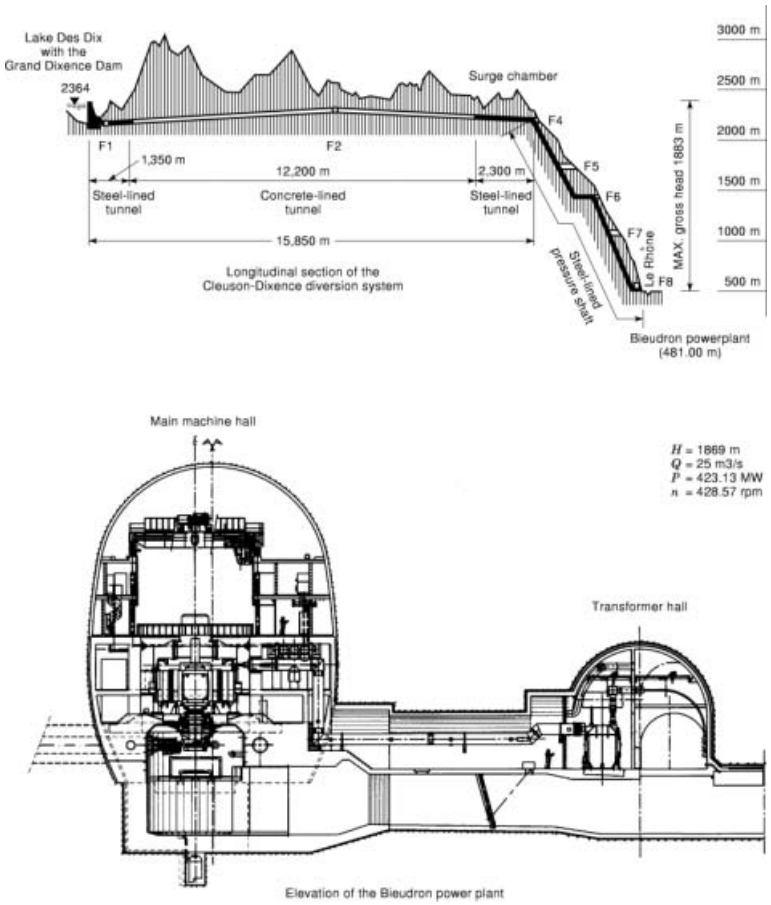

Fig. 3. Powerhouse at a great distance from the dam: large vertical Pelton turbine, Bieudron (Switzerland).

Design Criteria for the Turbine. This short subsection gives the main guidelines for the design and selection of the turbine. The turbine design is essentially based on the following criteria:

- Rated output P_t (MW)
- Net head H_n (m)
- Rated discharge Q_n (m^3/s)
- Rated speed n_n (rpm)
- Operation ranges such as the minimum and maximum head, the minimum and maximum output power, and the suction head

An important concept when choosing turbines and comparing their performance is that of the specific speed n_q. This allows turbines to be classified into two categories, slow or fast, on the basis of the relation between their hydraulic head, their rotational speed, and their output. The specific speed n_q is a characteristic constant valid for all machines geometrically similar to those being considered, and is given by the following

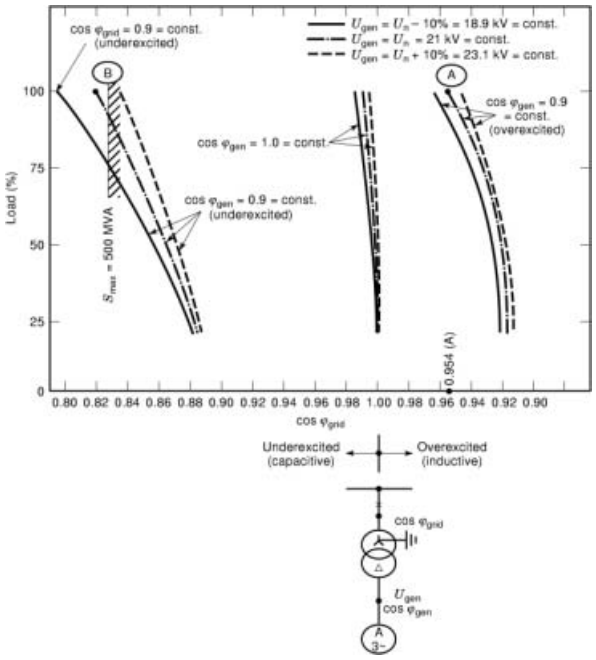

Fig. 4. Power factor at the network side as a function of the load (%) of the step-up transformer, Bieudron powerplant, Switzerland, for various power factors at the generator terminal. For example, for point A, the data are as follows: 100% transformer load (465 MVA); generator voltage $U_{ng} = 21$ kV; power factor cos ϕ of the generator terminals, 0.9 (overexcited); power factor of the network side, 0.954 (inductive). For point B, the data are as follows: 100% transformer load (465 MVA); generator voltage $U_{ng} = 21$ kV; power factor cos ϕ of the generator terminals, 0.9 (underexcited); power factor of the network side, 0.82 (capacitive).

relationship:

$$n_q = n \cdot \frac{Q_n^{1/2}}{H_n^{3/4}}$$

Turbine designers have to design machines that will operate with the best output possible. When setting up a project for a new turbine, it is possible to choose a reference model on the basis of a calculation of n_q which has been carried out as a function of n, Q, and H. Slow machines (small n_q) are used for large hydraulic heights and small discharges, whereas fast machines (large n_q) are used for small heads and large discharges.

Turbines can be classified as follows, according to their specific speed n_q and head H:

$350 < H < 1800$ m,	$2 < n_q < 20$:	Pelton
$40 < H < 700$ m,	$18 < n_q < 120$:	Francis
$5 < H < 80$ m,	$70 < n_q < 400$:	Kaplan

The optimum model efficiency or best point efficiency, for a Francis turbine (see Fig. 9), is reached for $n_q = 55$ to 70 with $\eta_{m\Lambda} = 0.94$. Taking into consideration the scale effect for $\Delta\eta = 0.015$ to 0.020, we obtain corresponding turbine efficiencies $\eta_{t\Lambda} = 0.955$ to 0.960.

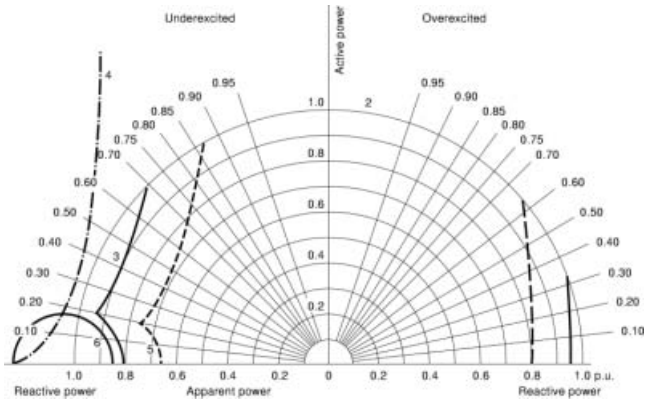

Fig. 5. Load diagram for the 465 MVA units, Bieudron power plant, Switzerland: 21,000 V, three phase, 50 Hz, 428.6 rpm, cos $\phi = 0.9$. Limits: 1, maximum excitation current, 3800 A; 2, stator current; 3, practical stability; 4, theoretical stability; 5, minimum excitation current; 6, circle of reactance. Voltage: solid curve, 1.0 p.u.; long-dashed curve, 1.1 p.u.; short-dashed curve, 0.9 p.u., where 1 p.u. = 465,000 kVA.

The phenomenon of cavitation, or the formation of pockets of vapor within a liquid, can only be harmful to the turbine. Besides the noise, the vibrations, and the losses of output caused by cavitation, it should be above all noted that solid material is attacked, an effect referred to as cavitation erosion. Cavitation, if it spreads, can compromise the correct functioning of the machine and also its service life.

With the aim of avoiding the problem, trials have been carried out in laboratories with the object of determining the degree and the type of cavitation. The trials determined the coefficient of cavitation σ, or Thoma coefficient. In practice, two coefficients are determined: the critical coefficient σ_c, which determines the start of cavitation, and the installation coefficient σ_i, which determines the direction of installation of the turbine in order to avoid cavitation. In all cases, $\sigma_i > \sigma_c$.

To illustrate the main characteristics of a turbine, the Itaipu turbine (Brazil) is given as an example:

$$
\begin{aligned}
P_t &= 740\,\text{MW} \\
H_n &= 118.4\,\text{m} \\
Q_n &= 677\,\text{m}^3/\text{s} \\
n_n &= 90.91\,\text{rpm} \\
n_q &= 65.9 \\
K &= n_q\sqrt{H_n} = 717 \\
\eta_t &= 0.955 \\
\sigma_c &= 0.436(n_q/157.7)^{1.388} = 0.13 \\
\sigma_{i\,\min} &= 0.137 > \sigma_c \qquad \text{(without cavitation)} \\
\sigma_{i\,\max} &= 0.764 \\
D_{1e} &= 8.1\,\text{m} \qquad \text{(outlet runner diameter)} \\
v &= 13.1\,\text{m/s} \qquad \text{(outlet water velocity at } Q_n\text{)} \\
D_{sp} &= 9.64\,\text{m} \qquad \text{(spiral inlet diameter)} \\
\Delta Z_d &= 3D_{1e} \qquad \text{(draft tube depth)}
\end{aligned}
$$

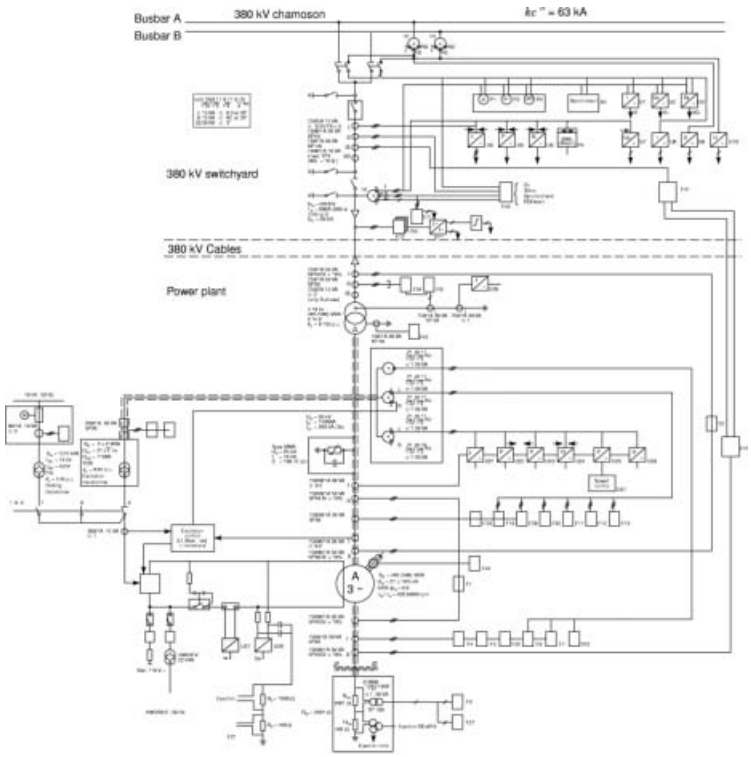

Fig. 6. Single-line diagram, Bieudron power plant, Switzerland: Excitation, measurement, and protection layout.

For the other types of turbines, such as Pelton, Kaplan, and bulb, a design optimization should be performed in each case with respect to:

- Choice of the rated and runaway speeds
- Expected weighted efficiency
- Cavitation damage as a function of the operating range
- Available suction head (for Kaplan and bulb turbines)

Finally, two coefficients have been defined by the turbine designers, which are used to characterize the machine behavior. These are the discharge coefficient ϕ_{1e} and the energy coefficient Ψ_{1e}, which can be formulated as follows:

$$\varphi_{1e} = \frac{Q_n}{\pi w R_{1e}^3} \approx 24.32 \frac{Q_n}{n_n \cdot D_{1e}^3}$$

$$\Psi_{1e} = \frac{2E}{w^2 R_{1e}^2} = \frac{2gH_n}{w^2 R_{1e}^2} \approx 729.5 \frac{gH_n}{(n_n D_{1e})^2}$$

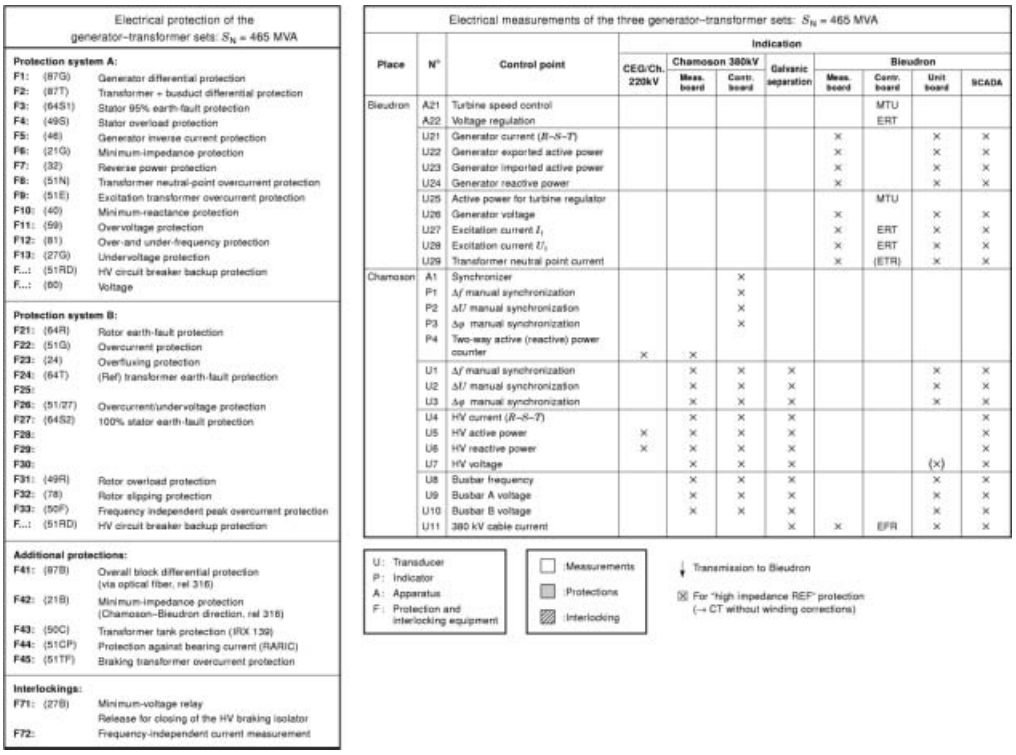

Electrical protection of the generator–transformer sets: S_N = 465 MVA

Protection system A:

F1:	(87G)	Generator differential protection
F2:	(87T)	Transformer + busduct differential protection
F3:	(64S1)	Stator 95% earth-fault protection
F4:	(49S)	Stator overload protection
F5:	(46)	Generator inverse current protection
F6:	(21G)	Minimum-impedance protection
F7:	(32)	Reverse power protection
F8:	(51N)	Transformer neutral-point overcurrent protection
F9:	(51E)	Excitation transformer overcurrent protection
F10:	(40)	Minimum-reactance protection
F11:	(59)	Overvoltage protection
F12:	(81)	Over-and under-frequency protection
F13:	(27G)	Undervoltage protection
F...:	(51RD)	HV circuit breaker backup protection
F...:	(60)	Voltage

Protection system B:

F21:	(64R)	Rotor earth-fault protection
F22:	(51G)	Overcurrent protection
F23:	(24)	Overfluxing protection
F24:	(64T)	(Ref) transformer earth-fault protection
F25:		
F26:	(51/27)	Overcurrent/undervoltage protection
F27:	(64S2)	100% stator earth-fault protection
F28:		
F29:		
F30:		
F31:	(49R)	Rotor overload protection
F32:	(78)	Rotor slipping protection
F33:	(50F)	Frequency independent peak overcurrent protection
F...:	(51RD)	HV circuit breaker backup protection

Additional protections:

F41:	(87B)	Overall block differential protection (via optical fiber, rel 316)
F42:	(21B)	Minimum-impedance protection (Chamoson–Bieudron direction, rel 316)
F43:	(50C)	Transformer tank protection (IRX 139)
F44:	(51CP)	Protection against bearing current (RARIC)
F45:	(51TF)	Braking transformer overcurrent protection

Interlockings:

F71:	(27B)	Minimum-voltage relay Release for closing of the HV braking isolator
F72:		Frequency-independent current measurement

Electrical measurements of the three generator–transformer sets: S_N = 465 MVA

Place	N°	Control point	Indication							
			CEG/Ch. 220kV	Chamoson 380kV		Galvanic separation	Bieudron			
				Meas. board	Contr. board		Meas. board	Contr. board	Unit board	SCADA
Bieudron	A21	Turbine speed control						MTU		
	A22	Voltage regulation						ERT		
	U21	Generator current (R–S–T)					×		×	×
	U22	Generator exported active power					×		×	×
	U23	Generator imported active power					×		×	×
	U24	Generator reactive power					×		×	×
	U25	Active power for turbine regulator						MTU		
	U26	Generator voltage					×		×	×
	U27	Excitation current I_1					×	ERT	×	×
	U28	Excitation current U_1					×	ERT	×	×
	U29	Transformer neutral point current					×	(ETR)	×	×
Chamoson	A1	Synchronizer			×					
	P1	Δf manual synchronization			×					
	P2	ΔU manual synchronization			×					
	P3	$\Delta\varphi$ manual synchronization			×					
	P4	Two-way active (reactive) power counter	×	×						
	U1	Δf manual synchronization		×	×	×			×	×
	U2	ΔU manual synchronization		×	×	×			×	×
	U3	$\Delta\varphi$ manual synchronization		×	×	×			×	×
	U4	HV current (R–S–T)		×	×	×				×
	U5	HV active power	×	×	×	×				×
	U6	HV reactive power	×	×	×	×				×
	U7	HV voltage		×	×	×			(×)	×
	U8	Busbar frequency		×	×	×			×	×
	U9	Busbar A voltage		×	×	×			×	×
	U10	Busbar B voltage		×	×	×			×	×
	U11	380 kV cable current				×	×	EFR	×	×

U: Transducer
P: Indicator
A: Apparatus
F: Protection and interlocking equipment

Measurements
Protections
Interlocking

Transmission to Bieudron

For "high impedance REF" protection (→ CT without winding corrections)

Fig. 7. Excitation, measurement, and protection layout: explanatory sheet to Fig. 6.

with

$$w = \frac{\pi n_n}{30} = \text{angular speed} \qquad (\text{s}^{-1})$$

$$R_{1e} = \frac{D_{1e}}{2} = \text{outlet runner radius} \qquad (\text{m})$$

$$g = 9.806\,\text{m}\cdot\text{s}^{-2} = \text{acceleration due to gravity}$$

Figure 10 is a diagram of the efficiency gradient chart of $\Psi_{1e} = f(\phi_{1e})$, determined during a model test on the La Grande 4 turbine, Canada. This test was carried out at the IMHEF laboratory of the Swiss Federal Institute of Technology, Lausanne.

Design Criteria for the Screened Busbars. Linkages between generators and transformers are generally realized by means of screened busbars made from aluminium. In view of the power transmitted, this solution is economically the most cost-effective and the most reliable. Furthermore, with this system, electromagnetic fields external to the system are reduced by between 95% and 98%. Given the large sensitivity of computer screens to these interference fields, this advantage is important. Figure 11 shows the influence of the power on the aluminum weight used.

Influence of the Power on the Aluminum Weight Used. The aluminum cross section of a busbar is essentially determined by the current to be carried and by the permissible temperature rises. The total weight of a connection therefore depends on the current rating, the authorized temperature rises, and the length of the run.

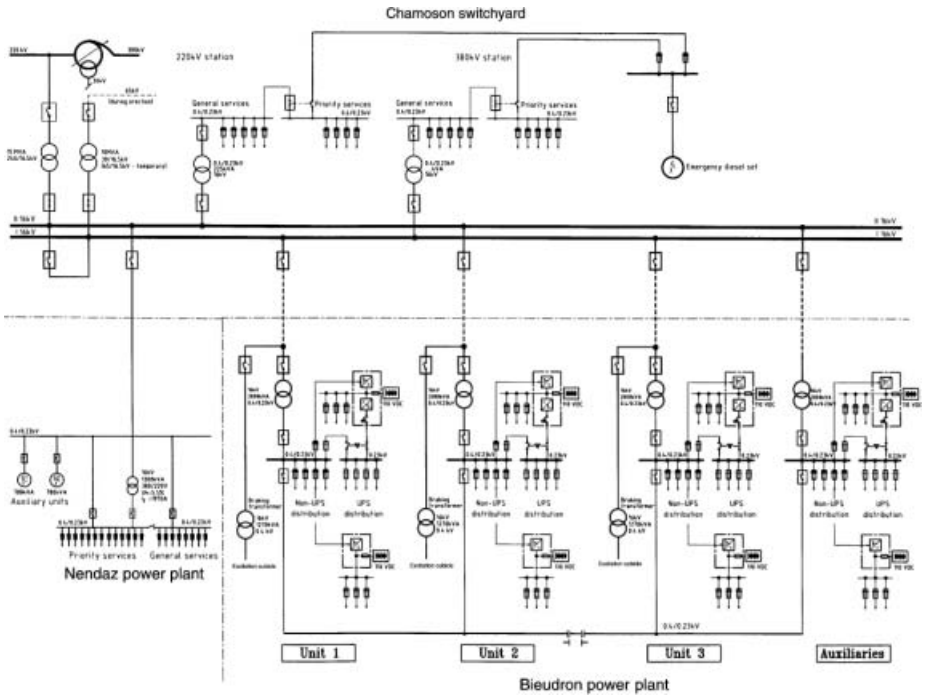

Fig. 8. Low-voltage installations and distributions: Bieudron power plant, Switzerland.

The graph in Fig. 11 is based on connections for which the temperature rises and the distances between the generator terminals and the transformer terminals are identical. This graph shows that the weight of aluminum used for the busbars increases linearly with the current and the power transmitted.

In fact, the busbar is self-cooled up to 600 MW. For identical temperature rises, the increase in power is reflected in a proportional increase in diameter, without a change in thickness. The increase in the busbar weight is therefore proportional to the power capacity. Beyond 600 MW, the busbar is cooled by forced ventilation. This ventilation significantly decreases the linear weight. For such units, however, the power is generally distributed by three single-phase transformers, and the bus must therefore contain an element that ensures the delta connection, which increases the busbar length. This increase in length compensates for the effect of the ventilation on the weight and, as a whole, the total busbar weight remains proportional to the power transmitted.

In practical terms, one 900 MW busbar uses as much aluminum as three 300 MW busbars.

Types of Conductors Having Metallic Protection. Designed in response to all the criteria above, and benefiting from long and profitable experience, conductors with metallic protection are characterized by:

- Hollow, rigid conductors supported by the insulators
- The use of air as a dielectric
- Sealed metallic protection, generally connected to earth at one end only

According to their degree of phase separation, conductors with metallic protection can be classified into the three types, described below.

Table 5. Large Vertical Pelton Turbines (H = 255 m to 1733 m)

Power Plant (Country)	No. of Units	Freq. (Hz)	Unit Capacity P (MW)	Net Head H (m)	Discharge Q (m^3/s)	No. of Jets	Rated Speed n (rpm)	Specific Speed[a] n_q	Hydr. Diam. D_1 (mm)	Commissioning Date
Bieudron (Switzerland)	3	50	423.30 393.60 370.90	1869.0 1733.0 1633.0	25.00	5	428.57	7.54 7.98 8.34	3993	1998–1999
Sellrain-Silz (Austria)	2	50	244.40 250.00 269.30	1154.9 1172.6 1233.1	23.70 23.90 24.50	6	500.00	12.29 12.20 11.89	2850	1982–1983
Jostedal (Norway)	1	50	266.00 288.00 301.00	1073.0 1131.0 1163.0	28.50	5	428.57	12.20 11.74 11.49	3175	1988
Guavio (Colombia)	5	60	202.00 224.80 260.80	961.0 1032.0 1140.0	23.60 24.40 25.70	5	450.00	12.67 12.21 11.63	2950	1992
Grand-Maison (France)	4	50	122.60 156.30 157.10	775.0 915.0 918.1	18.10 19.50 19.50	5	428.57	12.41 11.37 11.35	2700	1986
Pigai-Aoos (Greece)	2	50	105.00 110.00 115.20	633.0 652.0 677.0	18.55 18.83 19.10	6	428.57	14.63 14.41 14.11	2415	1990
La Batiaz (France)	2	50	98.00 102.80 103.50	621.0 648.0 652.0	17.60 18.00 18.15	5	428.57	14.45 14.16 14.15	2360	1983
Devil Canyon (USA)	2	60	70.96 76.06 89.77	362.1 381.0 423.7	22.08 22.65 23.89	6	276.90	15.67 15.28 14.49	2836	1992
San Agaton (Venezuela)	2	60	141.70 153.00 178.70	333.0 350.0 389.0	48.54 49.76 52.46	6	225.00	20.10 19.61 18.60	3330	1987
Restitution (Peru)	3	60	70.94 74.50 75.30	247.0 255.0 257.0	32.73 33.27 33.39	6	200.00	18.36 18.08 18.00	3210	1984–1985

Range	Minimum	Maximum
Rated unit capacity P (MW)	74.50	393.60
Rated net head H (m)	255.00	1733 (world record)
Rated specific speed[a] n_q	18.08	7.98

[a] $n_q = nQ^{1/2}H^{-3/4}$ (n in rpm, Q in m^3/s, H in m).

(1) Nonsegregated Phase Conductors Often referred to as *NSPB* (Nonsegregated phase bus). In the case of an installation in a confined space, the suppression of the metallic screen between the phases allows the space required by the three-phase installation to be reduced. When there is the risk of phase-to-phase short circuit and of extensive electrodynamic stresses, conductors with a large cross section then become necessary, as well as an increase in the number of insulators. In this case, the suppression of the screens does not generally result in a cost reduction, but limits the tendency to short circuit, and reduces the rigidity and the self-supporting characteristic of the linkage.

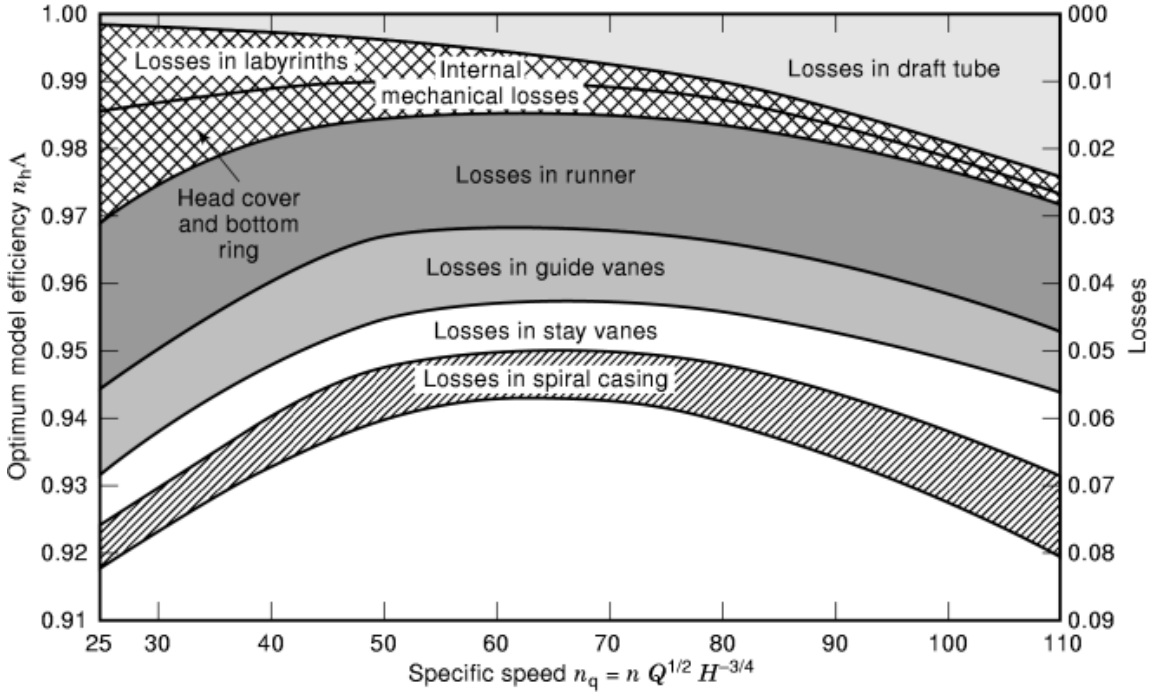

Fig. 9. Optimum model efficiency at full load (loss distribution) for Francis turbines.

(2) Isolated Phase Conductors Often referred to as *IPB* (isolated phase bus). Representing the top of the range, these are used for rated currents that can exceed 50 kA with rated voltages between 3.3 kV and 33 kV, and are generally cooled by closed-circuit forced ventilation above 20 kA. The set of three-phase conductors is composed of three rigid, hollow conductors (one for each phase), generally made of aluminum. Their three-phase design under a continuous casing connected together electrically at their ends allows them to withstand very high short-circuit intensities, even in the case of low rated currents, and ensures exemplary functional security. Each conductor is centered by means of the insulators in a circular sectional casing made of aluminum; this casing ensures a high degree of protection, allowing the quality of the dielectric (air) to be guaranteed, and preventing all access to the parts that are under voltage. Each casing is insulated from the adjacent casing by an air gap, which prohibits propagation of any phase-to-earth breakdown to the neighboring phases. Continuity being assured along the length of the casing, including the extremities, an induced current of an amplitude approaching that of the phase current, but in the opposite direction, results, which has the effect of canceling out the external magnetic field.

(3) Segregated Phase Conductors Often referred to as *SPB* (segregated phase bus). Using a technology much simpler than the preceding types, the segregated phase conductors provide a good compromise:

- A high level of security assured by the phase separation, a sealed metal casing, and air insulation
- Reduced space requirement. Their design makes them particularly suitable for rated currents between 1500 A and 5000 A at rated voltages between 3.3 kV and 33 kV.

A set of three-phase conductors consists of three rigid, hollow conductors, separated by a metallic screen, and supported by the insulators within a square-section casing common to the three phases. This casing is

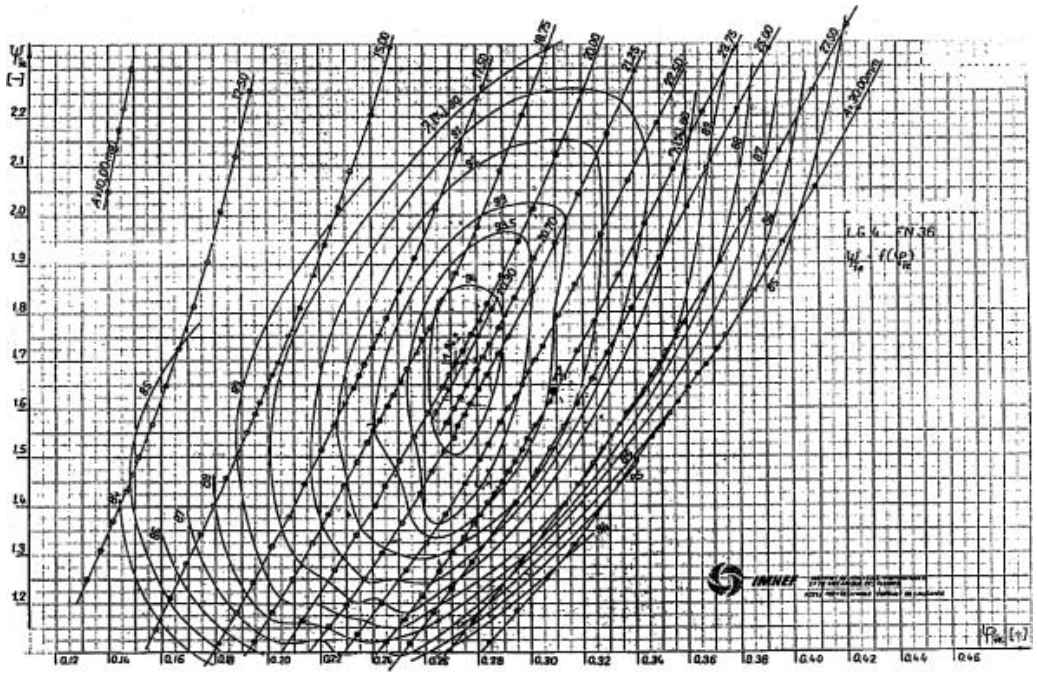

Fig. 10. Turbine model test results: the efficiency Hill chart, $\Psi^{-}{}_{1e} = f(\phi^{-}{}_{1e})$, measured on a model of the La Grande 4 turbine, Canada, during performance tests. The prototype rated data of this Francis turbine are $Q = 278\ \mathrm{m^3/s}$,, $D^{-}{}_{1e} = 5.55$ m, $H = 116.70$ m, $g = 9.80\ \mathrm{m \cdot s^{-2}}$, $n_n = 128.57$ rpm. After calculation we obtain $\phi^{-}{}_{1e} = 0.3076$, $\Psi^{-}{}_{1e} = 1.6385$ represented by point A. The resulting efficiency η_t at full load is given by $\eta_t = \eta_M + \Delta\eta = 92.6\% + 1.7\% = 94.3\%$. (Courtesy IMHEF, EPFL, Switzerland.)

made from aluminum in order to reduce the residual external magnetic field. It is designed to ensure a high degree of sealing, the metallic screens between the phases reducing the electrodynamic effect in the case of a short circuit, and increasing the rigidity and the self-supporting characteristic of the assembly.

According to the degree of separation of the phases and the type of protected conductor chosen, each of the three types of basic channeling has specific advantages, depending on the constraints applied and the technology used. The main routes are common to the three types.

Phase Conductors. The phase conductors are generally manufactured from aluminum with 99.5% purity (1050A or equivalent):

- Particularly in the case of insulated phases
- Preferably in the case of segregated or nonsegregated phases.

Its characteristics (conductivity, weight, ease of use, price) very often make this metal preferable to copper. It allows the realization of on-site welded junctions, which are necessary to guarantee optimal performance and total reliability of insulated phase conductors. In addition, advanced technologies permit the solution of the problems of electrical contact in detachable junctions.

The hollow conductors are made from extruded sections, which are folded or rolled, and welded. Their shape chosen to provide:

- A good distribution of the alternating current

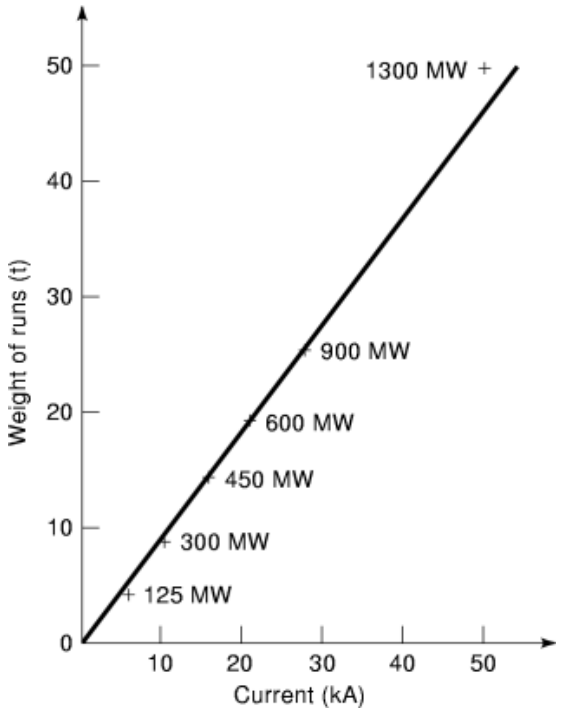

Fig. 11. Aluminum weight for ordinary runs as a function of the current.

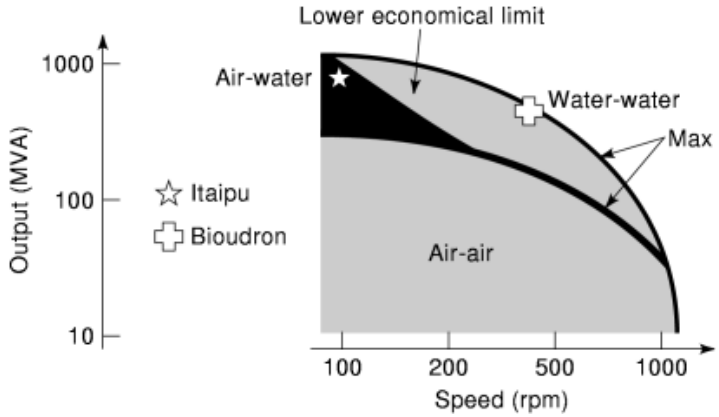

Fig. 12. Generator output versus speed (logarithmic scales). Diagram of the generator cooling mode in a plot of the output and speed, with two remarkable examples: the Itaipu generator (823 MVA; 90.91 rpm; water-cooled stator; air-cooled rotor), and the Bieudron generator (465 MVA; 428.57 rpm; fully water-cooled).

- A large emissive surface for the dissipation of heat
- High mechanical resistance in the case of a short circuit
- Rapid fixation of the insulators

In order to improve the caloric dissipation, the external surface of the conductor is sometimes painted matt.

Casing. The casing is always manufactured from aluminum with a purity of 99.5%—a nonmagnetic material with very high electrical conductivity—bringing the following advantages:

- A weak residual field to the exterior of the casing, thanks to the induced current, whose effect is in opposition to the magnetic field created by the conductors
- Reduced heating of the casing
- Increased rigidity, permitting a larger self-supporting characteristic for a low weight
- Circuit continuity to earth

A matt coat of paint applied to the interior of the casing will improve the absorption of heat emitted by the conductor and help in its dissipation.

The external surface is sometimes painted, in order to:

- Improve its appearance
- Take account of architectural needs or identification requirements
- Reinforce the protection against aggressive environments
- Facilitate the dissipation of heat

The casing, which provides effective protection of the parts under voltage, is mechanically reinforced at the fixation points of the insulators, and has anchorage points on the frame.

To facilitate installation and maintenance, inspection flaps are provided to the right of the detachable junctions and of the insulation supports. The very high degree of sealing that is always necessary is obtained by the utilization of welding in the manufacture of the casing, and by special precautions taken at junctions between elements and at the fixations of the inspection flaps.

This type of manufacture allows a continuous and homogeneous assembly to be achieved. An internal overpressure system can be added to improve the protection against the entry of fine dust.

Insulator Supports. The conductors are supported within the casing by insulators, which can be either of porcelain or of epoxy resin. These insulators are of the internal type, and can carry fins to improve dissipation. Their height is determined by the level of insulation that has to be ensured. At their base, they are fixed to the casing, which is reinforced for this reason. They support the conductor from the front to ensure that it remains in position, while allowing functional linear expansion to take place.

The characteristics of the insulators and their installation pitch are determined by:

- The permanent supporting stress
- The dynamic constraints resulting from short-circuit currents

Capacity of Protected Busbars. The formula generally used for calculating the maximum admissible current and the volume of the installation is the following:

$$I = 5kS^{0.8}p^{0.38}$$

where

I = current (A)
S = cross section of the conductor (mm^2)
p = external perimeter of the conductor (mm)

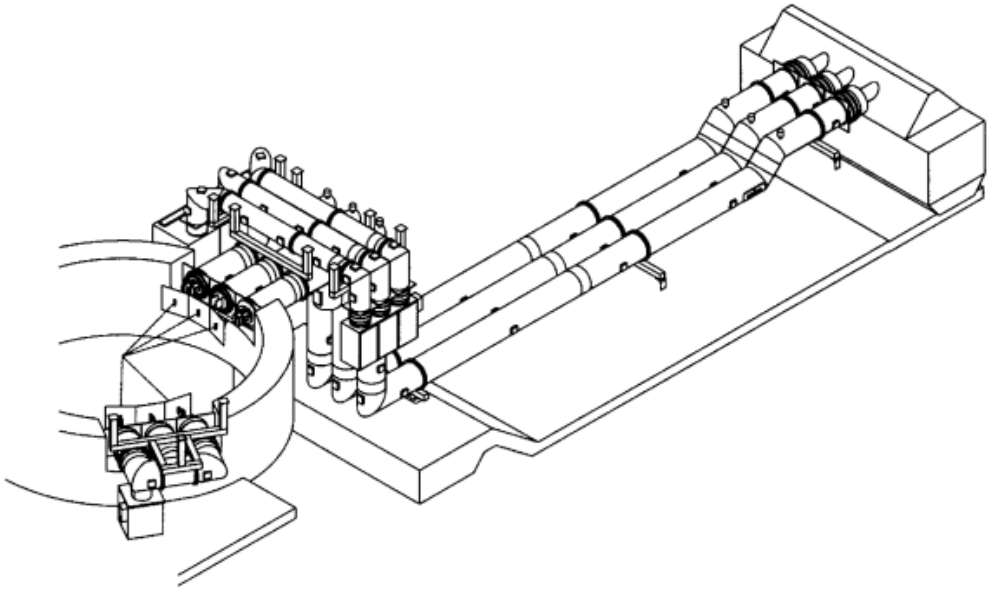

Fig. 13. Screened busbar, Bieudron power plant, Switzerland.

k = coefficient depending on the geometry of the system, the nature of the conductor, the number of parallel conductors, the working environment, the temperature rise, the conductor painting, the system frequency, and the ventilation mode; $k \approx 1$ to 6

An example of application of screened busbars is shown in Fig. 13, representing the 21 kV generator–transformer links of the Bieudron power plant, Switzerland.

Large Vertical Pelton Turbines

The use of a Pelton turbine must be considered as soon as the head of the installation becomes important. Table 6 shows the main large vertical Pelton turbines in service or being assembled throughout the world, classified according to their net head, which varies between 247 m (minimum) and 1869 m (maximum).

As soon as it comes into service, which is planned for the end of 1998, the Bieudron power plant in Switzerland will hold the world record for net head. The maximum net head will be 1869 m, with a discharge of 25 m^3/s, which will allow the turbine to provide 423.13 MW at 428.57 rpm (see Fig. 3).

The regulation of the output power of a Pelton turbine can be varied between 30% and 100% of its rated power as a function of the number of nozzles in service. The efficiency obtained in this way will be between 0.91 and 0.92, thereby remaining practically constant over the complete useful functional range of the machine (see Fig. 14, curve 1).

Within the same range of application, a Pelton turbine has some significant advantages over a Francis runner: the setting is not as deep as for a Francis unit, thereby requiring a smaller excavation volume; there is no hydraulic thrust; higher reliability results from the simpler design; and it offers easier and less expensive maintenance.

Table 6. Large Vertical Francis Turbines (Low Head: H = 50.8 m to 275.6 m)

Power Plant (Country)	No. of Units	Freq. (Hz)	Unit Capacity P (MW)	Net Head H (m)	Discharge Q (m^3/s)	Rated Speed n (rpm)	Specific Speed n_q	Thoma Coeff. σ (min/max)	Runner Outlet (mm)	Commissioning Date
Itaipu	9	50	400	82.9	545.0	90.91	77.2[a] 78.4[b]	0.137		
(Brazil/Paraguay)	9	50	740	118.4	677.0	92.31	65.9[a] 66.9[b]	0.764	8,100	1984–1991
			740	126.7	621.0		60.0[a] 60.9[b]			
Sayano-Shushenskaya	10	50	550	175.0	335.0			0.100		1978–1983
			650	194.0	360.0	142.86	54.3	0.200	6,250	
(Russia)			735	220.0	358.0		42.1 47.3			
Guri-II	10	60	476	111.0	472.0			0.123		
(Venezuela)			610	130.0	513.0	112.50	71.5	0.211	6,900	1978–1986
			787	146.0	585.0		66.2 64.8			
Revelstoke	6	60	370	110.0	384.2			0.119		1984–1988 (4)
(Canada)			467	126.8	419.4	112.50	64.9	0.157	6,121	1994 (2)
			495	130.2	436.2		61.0 61.0			
Piedra del Aguila	4	50	236	95.8	220.0			0.197		
(Argentina)			356	108.0	353.0	125.00	60.0	0.219	5,993	1991–1994
			375	114.2	353.0		70.0 67.2			
Tucurui (Brazil)	12	60	250	51.4	529.0			0.217		
			320	60.8	574.0	81.81	96.0	0.350	8,150	1986–1992
			389	67.6	598.0		90.0 84.8			
Itaparica (Brazil)	3	60	216	46.3	510.0			0.330		
			250	50.8	539.0	81.81	104.1	0.440	7,790	1988–1991
			264	53.2	542.5		99.8 96.7			
Alto Lindoso	2	50	215	218.6	108.7			0.167		
(Portugal)			317	275.6	126.0	214.29	38.6	0.215	3,770	1988–1989
			317	280.8	123.3		35.6 34.7			
Atatürk + Karakaya	8 + 6 = 14	50	245	125.0	215.4			0.108		
			306	152.0	217.5	150.00	59.3	0.165	5,150	1965–1995
(Turkey)			325	157.0	223.0		51.1 50.5			
Tarbela (Pakistan)	4	50	440	49.4 117.4	428.4	90.91	52.8	0.110 0.480	7,150	1993–1994
			440	135.6	375.0		44.3			
La Grande 4	9	60	295	115.5	277.0			0.130		
(Canada)			300	116.7	278.0	128.57	60.7	0.170	5,560	1984–1985
			307	118.6	280.0		60.4 59.9			
Three Gorges (TGP) (China)	26	50	700	80.6	950.0	75.00	86.0	N/A	10,000	2003–2009

Range	Minimum	Maximum
Rated unit capacity P (MW)	250.0	740.0
Rated net head H (m)	50.8	118.4
Rated specific speed n_q	99.8	65.9/66.9

[a] 50 Hz.
[b] 60 Hz.

Large Vertical Francis Turbines

Francis turbines can be installed for net heads that vary considerably, from about 50 m up to more than 700 m. In the case of pump–turbine power plants, the possibility of using the same machine for the two modes of operation (reversible group) has again increased the interest in Francis turbines.

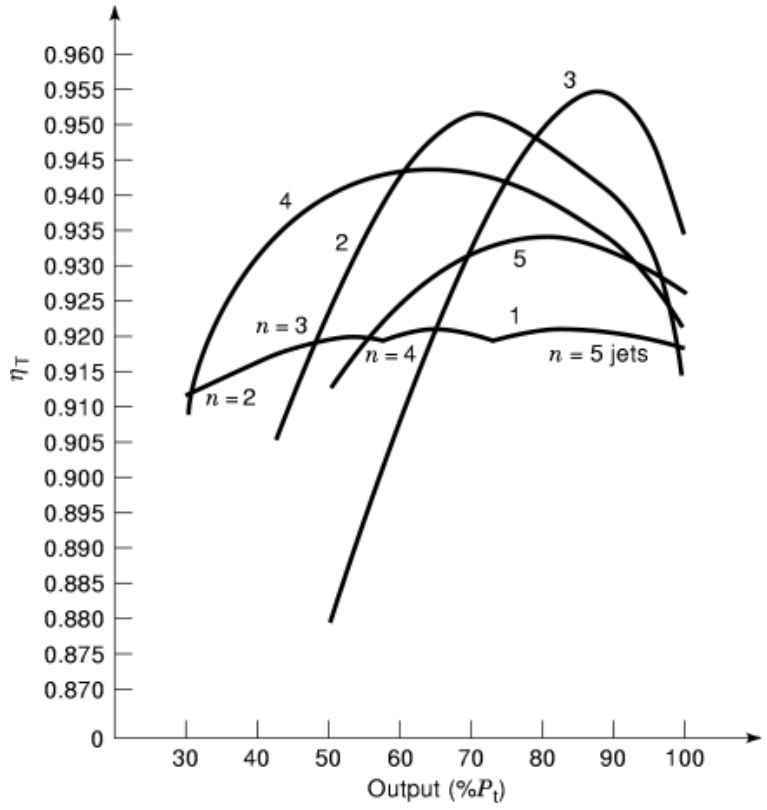

Fig. 14. Turbine Efficiency: Bieudron (Pelton turbines), Switzerland, (P_n = 423.3 MW = 100% at H = 1869 m); Koyna IV (Francis turbines—high head), India (P_n = 316.6 MW = 100% at H = 500 m); Itaipu (Francis turbines—low head), Brazil–Paraguay (P_n = 740 MW = 100% at H = 118.4 m); Porto Primavera (Kaplan turbines), Brazil (P_n = 103.6 MW = 100% at H = 18.3 m); Tadami (bulb turbines), Japan (P_n = 65.8 MW = 100% at H = 19.8 m).

Table 7 lists the largest Francis turbines operating on a net head basis (50 m to 275 m) throughout the world.

The Itaipu power plant in Brazil is currently the largest such plant in operation in the world, with 18 units of 700 MW each, totaling 12,600 MW installed capacity. It has an earth fill dam 7760 m long and 196 m high, with a storage capacity of 29×10^9 m^3.

The Three Gorges Project (*TGP*) in China, which is now in the realization phase, will consist in the first stage (2003) of 14 groups of 700 MW each, and, when completed (2009), of 26 such groups. TGP will then hold, with 18,200 MW, the world record for installed power by a large margin. It is expected to generate an estimated 85 TWh per year.

The TGP presents several challenges for engineering design. The Francis turbines will be the largest in size in the world. The problems of installing and operating such large machines have already been experienced at Grand Coulee (USA) and Itaipu (Brazil–Paraguay). The first units will operate at an average head that is much lower than will be obtained when the dam is completed. It is a critical technical issue for stable operation and for the maximum efficiency of these units that they should be adaptable to work over the especially large net head (H_n) range of 61 m to 113 m.

Table 7. Large High-Head Francis Turbines and Pump–Turbines (Single Stage, H = 460 m to 733 m)

Power Plant (Country)	No. of Units	Type	Freq. (Hz)	Oper.	Unit Capy. P (MW)	Dischg. Q (m^3/s)	Net Head H (m)	Rated Speed n (rpm)	Spec. Speed n_q	Thoma Coeff. σ	Runner Outlet Diam (mm)	Commissioning Date
Tianhuangping (China)	6	P–T	50		338.0	61.0	610.0	500.00	3.0	N/A	2050	1997–1998
Häusling (Austria)	2	P + GM + T	50	T	166.5	32.5	568.0	600.00	29.1	0.109	1800	1988
					181.0	30.7	643.1		26.0	0.187		
					181.0	27.0	733.0		22.1			
Bajina Basta (Servia)	2	P–T	50	T	243.0	58.0	497.5	428.57	31.0	0.108	2180	1980–1981
					284.0	63.1	554.3		28.8	0.171		
					315.0	61.1	600.3		27.6			
					210.0	36.7	621.3		27.6	0.104		
				P	272.0	40.4	600.6		22.5	0.159		
					299.0	50.8	5331.7		20.9			
Chaira (Bulgaria)	4	P–T	50	T	171.0	34.0	578.0	600.00	29.8	0.106	3517	1992
					261.0	36.0	653.4		27.9	0.169		
					216.0	36.1	676.8		27.2			
				P	169.4	21.3	701.0		22.3	0.102		
					186.2	25.7	660.0		23.4	0.159		
					196.9	29.5	613.4		26.4			
Svartisen (Norway)	2	T	50	T	322.0	78.0	460.0	333.33	29.6	0.060	2354	1993
					350.0	71.5	543.0		25.0	0.053		
					386.0	73.0	585.0		23.9			
Koyna-IV (India)	4	T	50	T	289.0	67.9	475.0	375.00	30.4	0.045	2400	1998
					316.0	71.2	500.0		29.9	0.055		
					326.0	69.2	525.0		28.5			

Range	Minimum	Maximum
Rated unit capacity P (MW)	166.5	350.0
Rated net head H (m)	500.0	660.0
Rated specific speed n_q	0.045	0.187

The concrete gravity dam, located on the Yangtze river, is 2335 m long and 178 m high, with an annual runoff of 450×10^9 m^3. The TGP reservoir may eventually reach nearly 40×10^9 m^3, extending over 600 km in length and 1.1 km in width.

The current final cost is estimated at 30.9×10^9 US dollars, or approximately $1700 per kilowatt installed.

Large High-Head Francis Turbines

Table 8 gives an overview of the largest Francis pump–turbines in service today throughout the world, for the specific case of single-stage machines for large heads (460 m to 733 m).

The Häusling power plant in Austria holds the world record for net head for Francis turbines, with 733 m. The Chaira power plant in Bulgaria, with reversible pump–turbines, holds two world records, for pump operation with a maximum head of 701 m, and for turbine operation with a head of 676 m.

The specific speed n_q of these machines varies between 20.9 and 32.

It is interesting to note that the net head for these Francis turbines is already within the functional range of Pelton turbines. From this point of view, Fig. 14, curve 2, shows the output of a high-head Francis turbine (Koyna IV, India) as a function of the turbine output. The regulating range of this machine extends

Table 8. Large Vertical Kaplan Turbines (H = 18.3 m to 39.2 m)

Power Plant (Country)	No. of Units	Freq. (Hz)	Unit Capacity P (MW)	Net Head H (m)	Discharge Q (m^3/s)	No. of Runner Blades	Rated Speed n (rpm)	Specific Speed n_q	Runner Blade Diam (mm)	Commissioning Date
Caruachi (Venezuela)	12	60	188.0	38.0	560.0	5	94.74	145.2	7790	2003
Liga III (Sweden)	1	50	168.4	35.20	535.0	5	107.14	155.9	7500	1982
			181.7	39.00	518.0					
			182.6	39.20	516.0					
Gezhouba (China)	2	50	74.0	10.60	852.0	4	54.54	195.4	11300	1981–1988
			176.0	18.60	1030.0					
			176.0	27.00	714.0					
Yacyreta (Argentina, Paraguay)	20	50	138.0	19.50	704.0	5	71.43	191.1	9500	1994–1997
				21.30						
				24.10						
Limestone (Canada)	10	60	114.0	25.70	485.0	5	90.00	167.1	7938	1990–1992
			125.4	27.60	500.0					
			128.8	28.20	500.0					
Rocky Reach (USA)	7	60	108.9	28.04	430.0	5	90.00	153.2	7120	2002
Taquaruçu (Brazil)	5	60	78.8	17.70	486.0	5	85.71	191.4	7700	1993–1994
			103.0	21.90	511.0					
			110.0	26.70	443.0					
Porto Primavera (Brazil)	18	60	103.0	18.30	618.0	4	75.00	210.7	8600	1967

Range	Minimum	Maximum
Rated unit capacity P (MW)	103.0	181.7
Rated net head H (m)	18.3	39.0
Rated specific speed n_q	145.2	210.7

from approximately 45% to 100% of the rated turbine output. The best-point efficiency amounts to 0.95 at 70% output, and to 0.91 at rated output.

Figure 15 shows two sections of power plants equipped with Francis turbines: the Itaparica power plant in Brazil, equipped with three low-head turbines of 250 MW and net head 50.8 m for a discharge of 539 m^3/s, and the high-head Churchill Falls power plant in Canada, with 11 turbines of 483 MW and net head 312 m.

Large Vertical Kaplan Turbines

Table 9 shows a list of the largest Kaplan vertical turbines in service or in the course of construction throughout the world.

Two types of Kaplan turbines are manufactured, a first type with regulating runner blades and guide vanes, and a second, called the propeller type, with regulating guide vanes and fixed runner blades.

Kaplan turbines operate with good efficiency within a power range of 30% to 100% of rated output. This is shown in Fig. 14, curve 4, which represents the output of a Kaplan turbine in the Porto Primavera power plant (Brazil) as a function of the power output. Within the 30% to 100% range of output power shown, the efficiency of the turbine varies between 0.91 and 0.92, the best-point efficiency being 0.94 at $0.65P_t$. Figure 16a shows a section of the plant, which is equipped with Kaplan turbines, having 18 turbines of 103 MW, 18.3 m net head, and a discharge of 618 m^3/s.

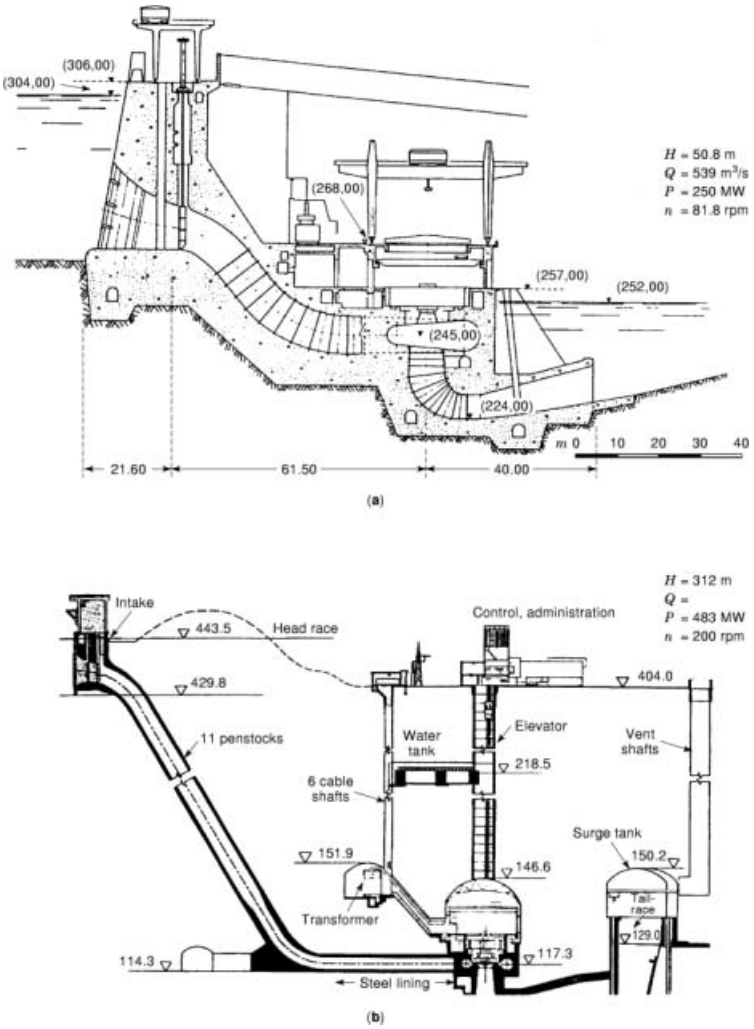

Fig. 15. Powerhouse close to the dam: (a) low-head Francis turbine, Itaparica (Brazil) (dimensions in meters); (b) medium-head Francis turbine, Churchill Falls (Canada).

The Kaplan turbine with the largest runner blade diameter currently in service is that of the Gezhouba power plant in China, which has a diameter of 11,300 mm for a power output of 176 MW at 18.60 m net head, with a discharge of 1030 m^3/s.

Large Bulb Turbines

Within the context of low-head hydroelectric installations, with heads between about 5 m and 20 m, the most suitable turbine types are bulb turbines, Straflo turbines, and S turbines. Table 10 lists some of these machines currently in service throughout the world.

Table 9. Large Bulb Turbines (Including Straflo and S; H = 5.33 m to 19.8 m)

Power Plant (Country)	No. of Units	Type	Freq. (Hz)	Rated Unit Capacity P (MW)	Rated Net Head H (m)	Rated Discharge Q (m^3/s)	Number of Runner Blades	Rated Speed n (rpm)	Specific Speed n_q	Runner Blade Diam (mm)	Commissioning Date
Tadami (Japan)	1	Bulb	50	52.00 65.80 65.80	17.00 19.80 20.70	338.0 366.0 358.0	5	100.0	219.6 203.8 196.0	6700	1989
Rock Island (USA)	8	Bulb	60	59.70 52.90	15.20 12.10	420.0	4	85.71	228.2 270.8	7400	–
Cakovec (Croatia)	2	Bulb	50	42.40	18.50	–	–	125.00	–	5400	–
Crestuma (Portugal)	3	Bulb	50	21.40 39.00 43.00	6.50 10.25 12.30	393.0 423.0 378.8	4	83.33	405.8 299.2 246.8	6800	1985–1986
Sloney A. Murray (USA)	8	Bulb	60	3.10 25.00 25.00	2.44 5.33 6.10	176.0 521.0 476.0	4	52.17	354.5 339.5 293.2	8200	1990
Greifenstein (Austria)	9	Bulb	50	20.70 34.40 46.50	7.00 10.90 15.05	350.0 360.0 335.0	4	93.75	407.6 292.4 224.6	6500	1984
Lock Dam (USA)	3	Bulb	60	10.60 24.30 25.00	4.57 8.41 8.99	295.0 329.0 395.0	4	90.00	494.6 330.6 307.7	61.00	1982–1983
Racine (USA)	2	Bulb	60	3.00 24.80 24.80	1.83 6.23 7.01	291.5 443.5 386.1	4	62.07	673.5 330.5 283.1	7700	1982
Laufenburg (Switzerland)	10	Straflo	50	8.20 11.00 11.60	7.20 9.50 9.97	132.0 129.0 131.0	4	107.14	225.0	4250	1994–1996
West End Dam (USA)	2	S-type	60	2.85 3.07 3.11	5.58 5.94 6.10	58.8 58.5 58.2	4	120.0	253.5 241.8 255.9	3210	–

Range	Minimum	Maximum
Rated unit capacity P (MW)	3.07	65.8
Rated net head H (m)	5.33	19.8
Rated specific speed n_q	203.80	339.5

Because of its smaller draft tube loss, the bulb turbine is more prone to cavitation than the usual Kaplan turbines. Its head is therefore limited to about 20 m. Another weak point of the bulb turbine is its nearly horizontal shaft. In the normal configuration of a directly coupled generator and a small admission hatch to the bulb through a vertical hollow rib, assembly and dismantling of the generator through a hatch at the downstream end of the bulb is difficult.

Because of their radially limited bulbs, bulb turbines with the generator inside the bulb have a rather small moment of inertia. This is not advantageous for stable regulation. In this respect, all tubular turbine designs that have the generator outside the water ducts are superior. These are, for example, the bulb turbine with bevel gear, the so-called S turbine, and, above all, the Straflo turbine.

Figure 16(b) shows the longitudinal section of one of the most powerful bulb turbines currently in service, that of Tadami, Japan, with a power of 65.8 MW, a net head of 19.8 m, and a discharge of 366 m^3/s. The

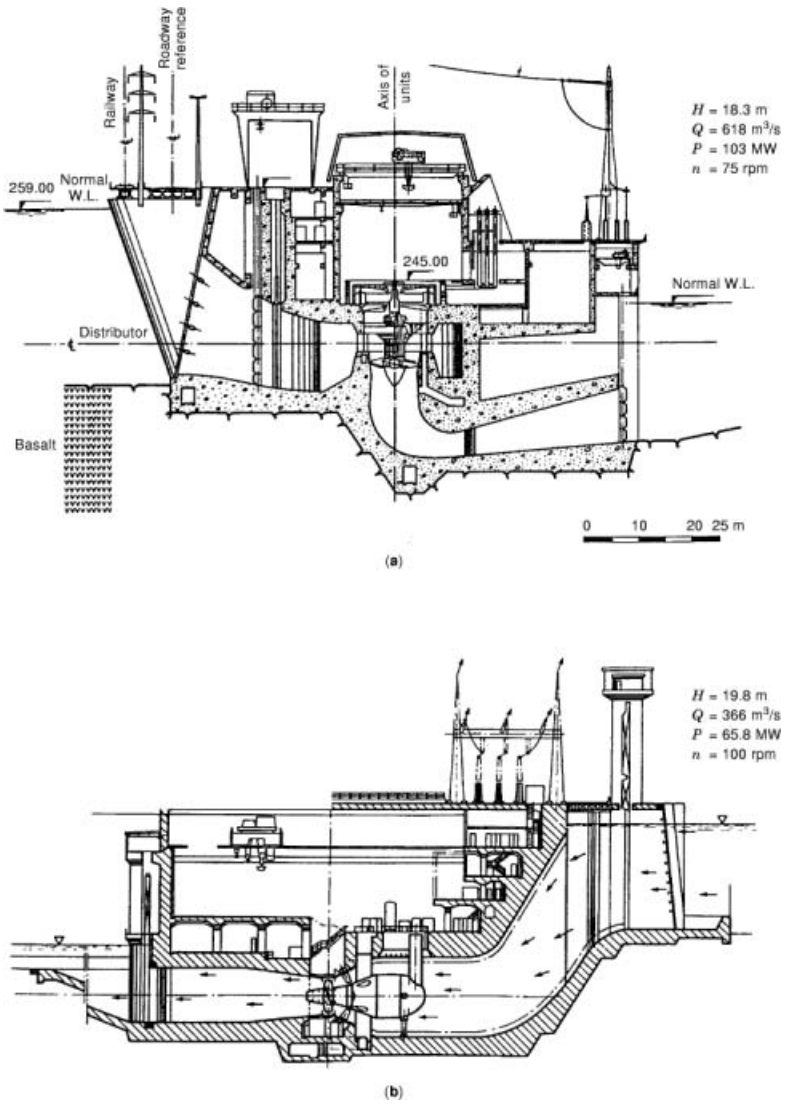

Fig. 16. Powerhouse within the dam: (a) Kaplan turbine, Porto Primavera (Brazil); (b) bulb turbine, Tadami (Japan).

efficiency of the Tadami bulb turbine is shown in Fig. 14, curve 5. When operating between 50% and 100% of its rated output power, it varies between 0.910 and 0.925, its best-point efficiency being 0.935 at $0.8P_t$.

World's Largest Vertical Generators

Table 11 shows the largest air-cooled generators currently in service throughout the world. The most powerful generator is that of the Grand Coulee power plant, in the United States, with a rated apparent power output of 826 MVA at 15 kV, and a rotation speed of 85.70 rpm.

Table 10. World's Largest Vertical Generators[a]

Power Plant (Country)	No. of Units	Freq. (Hz)	Rated Apparent Power (MVA)	Rated Power Factor cos φ	Rated Voltage U (kV)	Rated Speed n (rpm)	Specific Power per Pole (MVA/pole)
Grande Coulee, USA	3	60	826.0	0.95	15	85.70	9.83
Itaipu, Brazil-Paraguay	9	50	823.6	0.85	18	90.91	12.48
	9	60	737.0	0.95		92.31	9.45
Guri II, Venezuela	10	60	805.0	0.90	18	112.50	12.58
Sayano Shusmensk, Russia	10	50	711.0	0.90	16	142.86	16.93
Ertan, China	6	50	642.0	0.95	18	142.86	15.29
Krasnoyarsk, Russia	12	50	588.0	0.85	18	93.75	9.19
Churchill Falls, Canada	11	60	500.0	0.95	15	200.00	13.90
Cabora Bassa, Mozambique	15	50	480.0	0.85	16	107.14	8.57
Paulo Alfonso, Brazil	6	60	486.0	0.90	18	120.00	8.10
Revelstoke, Canada	4	60	485.0	0.95	16	112.50	7.58
Mica Creek, Canada	4	60	457.0	0.90	16	128.57	8.16
Bath County, USA	6	60	447.0	0.90	20	257.14	15.96
Guri I, Venezuela	4	60	414.0	0.85	18	128.57	7.39

Rated Power S_n (MVA)	Worldwide Units in Operation
300 to 400	230
200 to 300	440
165 to 200	320

[a] Air-cooled or evtl. water-cooled stator winding; S_n = 414 MVA to 823.6 MVA.

The largest power plant currently in service (1998) is that of Itaipu, with 18 installed machines, totaling 12,600 MW. This power plant was constructed straddling two countries, Brazil and Paraguay, which have different network frequencies of 60 Hz and 50 Hz respectively, and the generators had to be designed accordingly, some for 60 Hz at 92.31 rpm and the others for 50 Hz at 90.91 rpm.

Tables 12 and 13 show the main electrical and geometrical characteristics of the generators of the two largest power plants in the world: Three Gorges, China, 18,200 MW, completion date 2009, and Itaipu, Brazil, 12,600 MW, completed in 1991.

Large Generator–Motors

Table 14 gives a list of the main large generator–motors in service in reversible pump–turbine power plants. These synchronous machines are of a classical design, with bearings that permit the machinery to be operated with two directions of rotation.

In pump mode there are two ways of starting the sets:

(1) With dewatered runner:

- Using a static frequency converter
- With indirect asynchronous starting at rated stator current, by inserting additional reactance or a starting transformer in the motor line
- With a pony motor directly coupled to the pump–motor set

Table 11. Main Generator Characteristics of the Three Gorges Units[a]

Number of Units	26
Rated frequency f	50 Hz
Transmission system	HVDG–EHV, ac
Rated apparent output S_n	777.80 MVA
Maximum continuous apparent output S_{max}	840 MVA
Rated voltage U_n	210 kV
Rated current I_n	22454 A
Rated power factor cos φ	0.90
Rated speed n_n ($2p = 80$)	75 rpm
Runaway speed n_r	150 rpm
Moment of inertia J	112,500 t · ^{2}
Rated efficiency at cos $\varphi = 0.9$ (overexcited)	≥98.77%
x_{dIn}	≤0.9 p.u.
x'_{dIn}	≤0.324 p.u.
x''_{dUn}	≥0.2 p.u.
Utilization coefficient[b] at rated output, C	9.95 kVA/m^3 · rpm
Cooling system hot-spot temperatures:	
Stator winding (cooled with demineralized water)	65°C
Field winding (cooled with air)	85°C
Stator core (cooled with air)	60°C
Stator bore diameter D	18,800 mm
Stator stacking height L	2950 mm
Diameter over coolers, D_e	21,230 mm
Pit diameter D_p	25,000 mm
Total height H	7600 mm
Rotor mass G_r	2000 t
Stator mass G_s	710 t
Generator mass G_{TOT}	3350 t
Turbine rotor mass G_{RT}	550 t
Hydraulic thrust F_{HT}	25,500
Thrust bearing load F_{TL}	47,500 kN
Specific mass at rated output	4.31 kg/kVA
Specific rated output per pole	9.72 MVA

[a] Water-cooled stator, air-cooled rotor; Francis turbines.
[b] Esson coefficient $C = S_n/D^2Ln_n$.

Table 12. Main Generator Characteristics of the ITAIPU Units[a]

Number of Units	9	9
Rated frequency f (Hz)	50	60
Transmission system	HVDC/EHV-AC	EHV-AC
Rated apparent output S_n (MVA)	823.6	737
Maximum continuous apparent output S_{max} (MVA)	823.6	766
Rated voltage U_n (kV)	18	18
Rated current I_n (A)	26417	23639
Rated power factor cos φ	0.85	0.85
Rated speed n_n (rpm)	90.91	92.31
Number of poles, $2p$	66	78
Runaway speed n_r (rpm)	170	170
Moment of inertia J (t · m^2)	82000	80000
Rated efficiency at cos φ = 0.9 (overexcited)(%)	>98.52	>98.64
x_{dIn}(p.u.)	≤0.9	≤0.9
x'_{dIn}	≤0.32	≤0.3
x''_{dUn}	≥0.2	≥0.2
Utilization coefficient[b] at rated output, C (kVA/m^3 · rpm)	10.11	9.57
Cooling system hot-spot temperatures (°C)		
Stator winding (cooled with demineralized water)	70	70
Field winding (cooled with air)	100	100
Stator core (cooled with air)	70	70
Stator bore diameter D (mm)	16000	16000
Stator stacking height L (mm)	3500	3260
Diameter over coolers, D_e (mm)	19730	19730
Pit diameter D_p (mm)	22000	22000
Total height H (mm)	6400	6400
Rotor mass G_r (t)	2050	2050
Stator mass G_s (t)	690	610
Generator mass G_{TOT}(t)	3550	3380
Turbine rotor mass G_{RT}(t)	450	450
Hyraulic thrust F_{HT}(kN)	15700	15700
Thrust bearing load F_{TL}(kN)	40200	39200
Specific mass at rated output (kg/kVA)	4.31	4.59
Specific rated output per pole (MVA)	12.48	9.45

[a] Air-cooled generators; Francis turbines.

[b] Esson coefficient $C = S_n/D^2 L n_n$.

Table 13. Large Generator–Motors (Air-Cooled) for Pump Storage Plants (S_n = 230 MVA to 438 MVA)

Power Plant (Country)	No. of Units	Turbine Type	Freq. (Hz)	Rated Apparent Power (MVA)	Rated Power Factor cos φ	Rated Voltage (kV)	Rated Speed (rpm)	Spec. Power per Pole (MVA)	Order (O) Commissioning (C) Year
Dinorwic, UK	6	P–T	50	330.0	0.9	18.00	500.00	27.50	1982 (C)
Guang Zhou, China	4	P–T	50	333.0	0.9	18.00	500.00	27.75	1994 (O)
Muju, Korea	2	P–T	60	371.0	0.9	18.00	450.00	23.19	1991 (O)
Mingtan, Taiwan	6	P–T	60	300.0	0.9	16.50	400.00	16.67	1989 (O)
Sanchong, Korea	2	P–T	60	438.0	0.9	18.00	360.00	21.90	1994 (O)
Dlouhe Strane, Czech Rep.	2	P–T	50	355.2	0.9	22.00	428.57	25.37	1994 (C)
Ohkawachi[a], Japan	1	P–T	60	395.0	0.85	18.00	360 ± 8.3%	19.75	1994 (C)
Okukiyotsu 2[a], Japan	1	P–T	50	345.0	0.9	16.50	428.57 ± 5%	24.64	1993 (C)
Vianden 10, Luxemburg	1	P–T	50	230.0	0.9	15.75	333.33	12.78	1993 (C)

[a]The two installations in Japan are of a new design with adjustable speed n_0 (±5% to 8%) for adjustable power, quick power response, and improvement of turbine efficiency. The generator rotors have three-phase distributed windings supplied by three-phase cycloconverters.

(2) With fully watered runner:

- direct asynchronous starting at 2.5 to 3 times the rated stator current, depending on the short-circuit power of the feeding network (example: Vianden 10 power plant, Luxembourg, and Capljina power plant, Bosnia and Herzegovina, with 230 MW to 250 MW generator–motors)

It should be noted, however, that a new type of machine that allows working at variable speeds has recently been developed and put into service in Japan, in the Okukiyotsu 2 and the Ohkawachi power plants. These new systems provide certain advantages, such as the possibility of adjusting the speed in turbine- or pump-mode operation as a function of the head, of making rapid changes of power, and of improving the output of the turbines or input power of the pump for optimum efficiency. The speed can be varied between ±5% and ±8% around the rated speed.

The variable-speed machine is excited with an ac field, which is supplied by a three-phase cycloconverter. The rotor is smooth, with three-phase distributed rotor windings. By varying the frequency of the field, the machine speed can be varied. One can also control the active power quickly by changing the angle between the field poles and the stator poles with excitation control.

Fully Water-Cooled Generators

Because of the increasing power of hydroelectric machinery with high rated speeds (>300 rpm), and in order to take into account the mechanical, thermal, and geometrical dimensional constraints (such as the diameter of the rotor, the height of the laminations, and the mass and the speed of rotation), it becomes increasingly necessary for generators to have their stator and rotor windings fully cooled by demineralized water, which allows their copper losses to be removed in a very effective way, while at the same time reducing the operational temperature at full power.

In this way, the dimensional constraints can be more closely respected, with, however, a greater complexity in the design of these machines. Limiting the temperature rise of these generators to values lower than those of classic air-cooled generators also allows the service life of these machines to be extended.

Table 14. Fully Water-Cooled Generators with Demineralized Water in Stator and Rotor Windings (S_n = 190 MVA to 465 MVA)

Power Plant	Rated Power: Apparent, S (MVA)	Rated Power: Active, P (MW)	$\cos\varphi$	Speed (rpm): Rated, n	Speed (rpm): Runaway, n_r	Rated Voltage u (kV)	Apparent Power per Pole (MVA)	Synchr. React. x_d (p.u.)	Trans. React. x_{dtn} (p.u.)	Moment of Inertia J (t · m²)	Time Constant[a] τ_J (s)
Tonstadt 1 (Norway)	4 × 190	4 × 161.5	0.85	375	600	12.0	11.88	1.00	0.32	750	7.16
Aurland (Norway)	2 × 250	2 × 225.0	0.90	375	645	15.5	15.63	1.00	0.30	1025	7.02
Oksia (Norway)	4 × 240	4 × 206.4	0.86	375	595	15.5	15.00	1.30	0.32	800	5.96
Sima (Norway)	2 × 370	2 × 318.2	0.86	300	520	20.0	18.50	1.15	0.32	2200	7.01
Kvilldal (Norway)	4 × 360	4 × 309.6	0.86	333.33	515	19.5	20.20	1.30	0.32	1625	6.39
Silz (Austria)	4 × 320	4 × 240.0	0.75	500	950	17.5	26.67	1.37	0.38	625	7.14
Bieudron (Switzerland)	3 × 465	3 × 418.5	0.90	428.57	800	21.0	33.21	1.15	0.35	1500	7.30
Tonstadt 2 (Norway)	1 × 360	1 × 309.6	0.86	300	515	17.5	18.00	1.15	0.32	2250	7.12
Swartisen (Norway)	1 × 410	1 × 352.6	0.86	333.33	560	21.0	22.78	1.10	0.32	2025	7.00

[a] $\tau_J = (J\omega^2/P_n) \times 10^{-3}$ s (J in kg · m², P_n in kilowatts); $\omega = (\pi n/30)$ s^{-1}.

Table 15 lists a number of generators that are fully water-cooled. They are mainly in operation in Norway, Austria, and Switzerland.

Table 5 shows the main electrical and geometrical characteristics of the Bieudron generator, in Switzerland, the holder of the world power record per pole for this type of machine with, 35.7 MVA/pole.

World Electric Energy Production

In 1995, the total annual production of electric energy worldwide was 13,300,000 GWh (see Table 16). The portion provided by nuclear power plants and classical thermal and industrial power plants represents 10,840,000 GWh, or 81.5% of the total, the remainder, 18.5% or 2,460,000 GWh, being provided by hydroelectric power plants.

The environmental impact of hydroelectric power plants is, as a rule, generally less than that of thermal power plants. For example, they do not contribute to the increase of the greenhouse effect, responsible for the global rise of temperature on the surface of the earth (no gas pollution).

The mean global consumption of electricity is continually increasing. It reached 2418 kWh per inhabitant per year in 1995, with, however, notable differences between the industrialized and developing countries. Norway was the country with the largest consumption, 26,000 kWh per inhabitant per year, while Burkina Faso was the lowest, with only 18 kWh per inhabitant per year.

Table 17 shows those countries that had hydroelectric energy production of more than 10,000 GWh in 1988.

Determination off the Basic Data for a Hydrostorage Plant

In the case of a water-storage installation, it is possible to determine the net electric energy produced by a power plant if one knows the useful volume of the storage reservoir (V_u) and the average net head (H_{av}).

Table 18 represents the annual inflow of water as a function of the aggregated hours (8760 hours per year). The volume of water in the reservoir that is not used is omitted, thus leaving the useful volume (V_u), shown by the cross-hatched surface *OABC,* from which the average annual output Q_{av} can be obtained.

Table 15. World Electric Energy Production

Region	Technically Feasible Hydropower Potential (GWh/y)	Economically Feasible Hydropower Potential (GWh/y)	Production from Hydropower Plants (GWh/y)	Installed Hydropower Plant Capacity (MW)
Asia	6,800,000	3,600,000	708,100	192,457
Europe	1,225,000	800,000	524,970	158,151
North and Central America	1,500,000	1,100,000	668,300	153,193
South America	2,600,000	2,300,000	450,100	97,053
Africa	1,665,000	1,000,000	67,000	20,512
Australia and Oceania	270,000	105,000	41,530	12,751
World total	14,060,000 (100%)	8,905,000 (63.3%)	2,460,000 (17.5%)	634,147

(b) World Total Electric Energy Production per Year

- Thermal and nuclear power plants (including industrial power plants): $E_t = 10{,}840{,}000$ GWh/yr (81.5%)
- Hydropower plants: $E_h = 2{,}460{,}000$ GWh/yr (18.5%)
- Total: $E = 13{,}300{,}000$ GWh/yr (100%)

(c) World Average Electric Energy Consumption

Per capita and per year, with population $C = 5.50$ billion

$$e = \frac{E}{C} = \frac{13{,}300{,}000 \times 10^6}{5.50 \times 10^9} = 2418 \text{ kWh/yr}$$

Country with the highest energy consumption: Norway, 26,000 kWh/yr
Country with the lowest energy consumption: Burkina Faso, 18 kWh/yr

It is then possible to graphically determine the installed output Q_{inst} by extending the linear portion of the output/hours curve from point C in the direction of the surface representing the volume of unused water. The intersection of the straight line and the surface then gives Q_{inst}. The electrical design characteristics, namely the average net output P_{av} and the installed net output P_{inst}, setting the design of the turbine and generator, and finally the annual net energy produced, E_y, can then be calculated.

An example of the calculation is shown in Table 18, with the following results:

$$\begin{aligned} V_u &= 1200 \times 10^6 \,\mathrm{m}^3 \\ Q_{av} &= 38.05 \,\mathrm{m}^3/\mathrm{s} \\ Q_{inst} &= 65 \,\mathrm{m}^3/\mathrm{s} \\ H_{av} &= 495 \,\mathrm{m} \\ P_{av} &= 169.25 \,\mathrm{MW} \\ P_{inst} &= 289.10 \,\mathrm{MW} \\ E_y &= 1482.63 \,\mathrm{GWh/yr} \end{aligned}$$

Table 16. The World's Hydroelectric Resources[a]

		Pure Hydroelectric Power Plants								
		In Operation			Under Construction			Planned		
Country	Exploitable Potential (GWh/y)	Total Capacity (GW)	Small Capacity (MW)	Total Generation in 1988 (GWh)	Total Capacity (GW)	Small Capacity (MW)	Probable Average Annual Generation (GWh)	Total Capacity (GW)	Small Capacity (MW)	Probable Average Annual Generation (GWh)
Argentina	390,000	6.600	40.400	15,692	4.300	0.82	25,200	3.200	75.70	10,500
Australia	30,000	7.259	34.500	14,581	0.827	0.00	1,100	0.050	0.00	190
Austria	55,700	10.200	320.000	36,340	0.100	N/A	N/A	7.000	210.00	20,000
Brazil	1,194,900	47.347	100.000	213,378	21.022	40.00	134,221	15.436	180.00	69,756
Canada	592,982	57.731	<50	313,189	4.317	N/A	23,310	15.700	N/A	N/A
China	1,923,304	32.69	3874.8	109,177	16.735	N/A	66,940	50.000	N/A	213,500
Colombia	418,200	6.700	100.000	24,220	1.400	0.00	6,830	2.900	35.00	15,760
Finland	47,000	2.600	110.000	13,350	0.060	0.00	130	0.080	10.00	240
France	266,000	24.300	800.000	69,150	0.100	0.00	300	1.470	0.00	2,110
Germany (FRG)	99,000	3.559	416.000	19,342	0.060	N/A	400	N/A	N/A	N/A
India	2,637,800	17.293	52.000	54,555	12.000	79	N/A	N/A	N/A	N/A
Italy	341,000	13.200	1.032	40,783	0.600	3.00	900	1.500	10.00	4,700
Japan	717,600	20.250	N/A	87,384	0.920	N/A	2,663	11.610	N/A	40,476
Korea (DPR of)	N/A	4.600	N/A	29,100	N/A	N/A	N/A	N/A	N/A	N/A
Mexico	500,000	7.734	N/A	20,800	1.590	N/A	4,205	3.515	N/A	9,770
New Zealand	N/A	4.587	18.200	21,891	0.432	0.00	2,000	0.096	0.40	445
Norway	550,000	24.381	113.600	104,343	1.713	2.90	3,646	3.573	13.00	13,895
Pakistan	N/A	2.900	107.000	16,689	1.928	52.25	10,640	7.131	104.50	39,355
Peru	416,000	3.800	50.000	11,000	0.210	10.00	1,200	4.500	25.00	1,000
Portugal	70,000	3.090	23.000	12,168	0.600	N/A	N/A	N/A	N/A	N/A
Romania	70,000	4.640	N/A	12,590	N/A	N/A	N/A	N/A	N/A	N/A
Spain	150,350	15.220	350.000	35,143	0.660	N/A	738	0.690	N/A	1,300
Sweden	200,000	16.100	310.000	68,742	0.200	20.00	415	0.200	20.00	2,400
Switzerland	144,000	11.500	192.000	36,500	0.230	3.60	663	N/A	N/A	1,750
Turkey	432,986	6.200	12.000	27,450	4.700	N/A	15,517	16.500	N/A	48,970
USA	528,300	71.359	700.804	222,938	1.057	49.456	3,887	N/A	N/A	N/A
USSR	3,942,000	62.200	400.000	219,800	14.500	N/A	56,400	30.000	3200.00	120,000
Venezuela	440,000	11.000	1.000	34,203	8.000	1.00	40,000	9.000	2.00	46,000
Yugoslavia	118,000	6.648	119.000	24,391	0.356	N/A	1,278	2.178	NA	6,336

[a]Source: *Water Power & Dam Construction Handbook*, 1990. Only countries with total hydropower generation above 10,000 GWh in 1988 are included.

Available Capacity and Actual Daily Load for a Given Network

Table 3 shows a diagram of the power demand on the Swiss national network over a 24 h period. The evolution of the country's production, and the distribution between consumption and excess for export, is shown as a function of the time of day on September 15, 1993.

In this diagram, it appears that the Swiss network is characterized by electric energy produced mainly by hydroelectric run-of-the river and hydrostorage power plants, to the extent of 65.3% of the total production, while the remaining 34.7% is provided by nuclear and thermal power plants.

Certain factors and formulae commonly used in electric energy production are defined in the calculations in Table 3.

Table 17. Hydrostorage Plant: Example with High-Head Francis Turbine

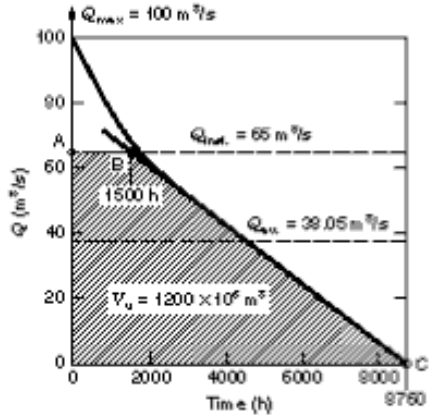

Useful volume V_u (area $OABC$):

$$V_u = \left(65 \times 1500 + \frac{65}{2} \times 7260\right) \times 3600 \approx 1200 \times 10^6 \text{m}^3$$

Average discharge Q_{av}:

$$Q_{av} = \frac{V_u}{8760 \times 3600} = \frac{1200 \times 10^6}{31.536 \times 10^6} = 38.05 \text{ m}^3/\text{s}$$

Installed discharge Q_{inst}:

$$Q_{inst} = 65 \text{ m}^3/\text{s} = 1.708 Q_{av}$$

Average net head $H_{av} = 495$ m.
Average net output P_{av} at H_{av}:

$$P_{av} = \rho g H_{av} Q_{av} \eta_t \eta_g \eta_{tr} \times 10^{-6} \text{MW}$$
$$= 997 \times 9.805 \times 495 \times 38.05 \times 0.94 \times 0.985 \times 0.995 \times 10^{-6} = 169.25 \text{ MW}$$

Installed net output:

$$P_{inst} = P_{av} \frac{Q_{inst}}{Q_{av}} = 169.25 \times \frac{65}{38.05} = 289.1 \text{ MW}$$

Net energy per year:

$$E_y = P_{av} \times 8760 \times 10^{-3} = 169.25 \times 87.60 \times 10^{-3} = 1482.63 \text{ GWh/yr}$$

or

$$E_y = \frac{\rho g \eta_t \eta_g \eta_{tr} V_u H_{av}}{3600} = \frac{997 \times 9.805 \times 0.94 \times 0.985 \times 0.995}{3600} V_u H_{av} \text{ GWh/yr}$$
$$\approx \frac{V_u H_{av}}{400} \approx 1485 \text{ GWh/yr}$$

where V_u is in units of 10^6 cubic meters, and H_{av} in meters.

The above calculations are based upon the following conditions:

- Water density at given temperature: $\rho = 997 \text{ kg/m}^3$ at $t_w = 25°\text{C}$
- Accelerationof gravity: $g = 9.805 \text{ m/s}^2$ at latitude 43° N
- Best point turbine efficiency at corresponding specific speed: $\eta_{t,\lambda} = 0.94$ at $n_{q\lambda} = 33$
- Generator efficiency: $\eta_g = 0.985$
- Transformer efficiency: $\eta_{tr} = 0.995$

The number of units ($n = 1, 2, 3, \ldots$) will be determined according to optimization and operation conditions.

Turbine Efficiency

The efficiency of turbines depends on the type of machine installed. Figure 14, curves 1 to 5, shows the efficiency of five different turbine types as a function of their output, where $100\%P_t$ corresponds to the rated turbine output.

It appears that the best point efficiencies are attained by medium- and high-head Francis turbines (curves 2 and 3), with values that can reach 0.950 (high head) to 0.955 (medium head). Their power range is normally between $50\%P_t$ and $100\%P_t$. These best-point values are slightly counterbalanced, however, by the relatively narrow power range of $70\%P_t$ to $90\%P_t$ within which they are achieved. To obtain a slightly lower efficiency, Kaplan turbines can be operated over a large output power range of between $30\%P_t$ and $100\%P_t$ (curve 4).

The Pelton turbine has a best-point efficiency that is lower than other types of turbines (curve 1), but has the advantage of being practically constant at 0.92 over the whole operating range of the turbine, between $30\%P_t$ and $100\%P_t$. The bulb turbines reach a best-point efficiency of around 0.935, and work with output powers between $60\%P_t$ and $100\%P_t$ (curve 5).

Itaipu Turbines

Figure 17 shows the field of operation specified for the Itaipu turbines as a function of the discharge and net head, with the corresponding power output curves. It is based upon the following requirements:

- The Paraguayan network can be energized by the Itaipu units, independent of the Brazilian network.
- The units can operate for long periods at close to no-load speed, either for test periods, or for generator warm-up prior to taking on load.
- The turbines can operate, for limited periods, at gate openings greater than those that correspond to the rated 715 MW. This overload region should extend to the maximum limit of 740 MW, which is imposed by the thermal restrictions of the generators.

The above requirements were to be met within the guaranteed limits on cavitation, vibration, and power fluctuations.

The *normal operation* range of the turbine was specified to be between 100% and 60% of the load at maximum normal gate opening, where both 50 Hz and 60 Hz units should be capable of continuous operation without restriction. Furthermore, the *overload* ranges with guaranteed maximum outputs were established as follows:

740 MW at 118.4 m net head
715 MW at 112.9 m net head
640 MW at 106.0 m net head

A *low-load operation* region was defined as being between 30% and 60% of the load corresponding to the maximum normal gate opening. Based on model tests, it was agreed that the low-load operation time should be limited to 5% of the total.

As the Paraguayan network can be energized by the Itaipu units independently of the Brazilian network, it was decided that three of the nine 50 Hz units could operate continuously, without restriction, in the region between 10% and 30% of the load corresponding to the maximum normal gate opening. This operating mode is

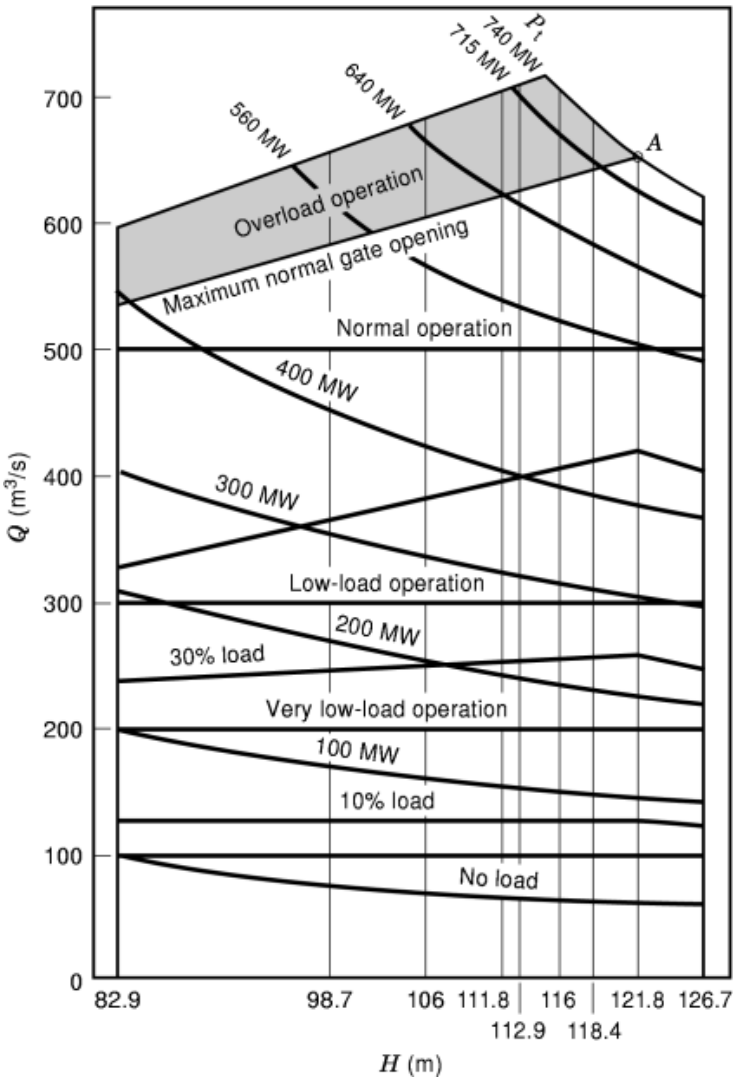

Fig. 17. Itaipu turbines: operating range.

referred to as *very low-load operation*. In order to meet this requirement, the following measures were taken with respect to the cavitation performance:

- Extension of the stainless steel protection on the suction side of the runner blades and band
- Continuous injection of air into the vaneless space between the runner and the wicket gates, through the head cover and the bottom ring.

Finally, to meet the requirements of test running, and to also preheat the generator before taking on load, it was agreed with the manufacturer that the turbine's guarantee was valid for up to 3% of the total operational time in the no-load speed region, at 10% of the load corresponding to maximum normal gate opening.

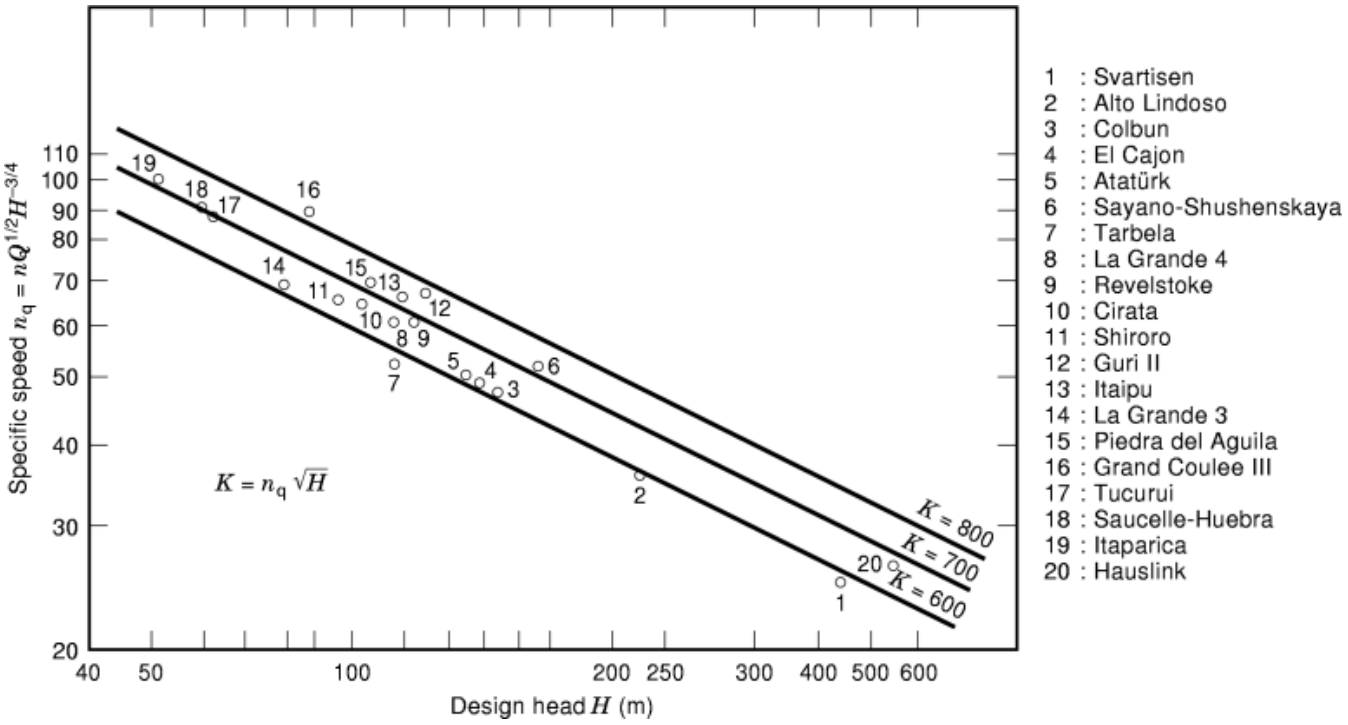

Fig. 18. Specific speed as a function of the design head (Francis turbines).

Turbine Efficiency

Knowledge of the efficiency of a turbine is important, since (as it varies with the discharge, net head, and specific speed n_q) it will be a determining factor in choosing the best functional range of the machine.

An example of the different model losses to be taken into consideration for the Francis turbine is given in Fig. 9. The losses are represented as a function of the specific speed n_q.

One can see that the best-point efficiency $\eta_{h\Lambda}$ is higher than 0.94 for a large range of specific speeds n_q, between 50 and 80. The optimum specific speed is around 60. In the case of Francis turbines operating under high heads with n_q varying between 25 and 35, the model efficiency ranges from 0.92 to 0.93.

This representation of the losses as a function of the specific speed is based on a scaled-down model, which allows the different components forming a Francis turbine (such as the runner, stay vane, guide vane, spiral casing, runner labyrinths, and draft tube), whose individual losses are also given as a function of n_q, to be designed in a better way.

Although turbines should always be operated under those hydraulic conditions that guarantee the best efficiency, certain operating limits exist and may not be transgressed. Namely, the operation of a turbine is first limited by the maximum guide vane opening, a second limit follows from the maximum power capacity of the generator, and a third limit is due to the cavitation index required.

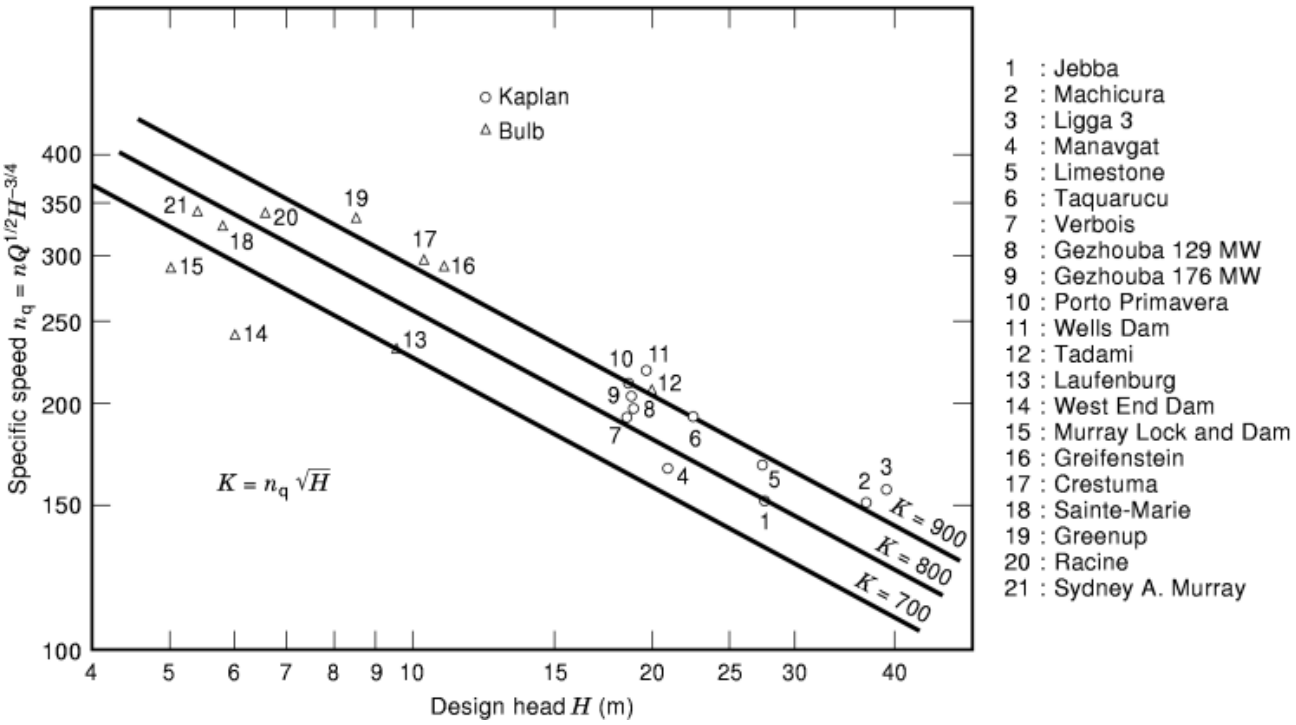

Fig. 19. Specific speed as a function of the design head (Kaplan and bulb turbines).

Speed Function

The choice of the unit's rated speed has an effect on the turbine and generator costs, on the turbine setting with respect to the tailwater level, and on the powerhouse costs. It may also be influenced by strength considerations, for example, in the case of an underground powerhouse where, because of favorable cavitation conditions, a higher rated speed could be selected, but may be limited by strength considerations.

The specific speed n_q of a turbine, defined as a function of the rated speed, net head, and discharge, is a fundamental value, which characterizes the machine's operational mode. It is a determining criterion for the optimization of the turbine design. A specific-speed diagram for Francis turbines is given in Fig. 18, and a diagram for Kaplan and bulb turbines is shown in Fig. 19.

Powerhouse Design with Respect to Distance from Dam

Powerhouses can either be built at a distance from the dam, as shown in Fig. 3, or close to or within the dam, as shown in Figs. 15 and 16.

(1) Powerhouses built at a distance from the dam usually incorporate a very long diversion section in the form of a channel, or an extended system of tunnels, penstocks, or pressure shafts. The powerhouse may be an open-air building at the end of the channel, or be linked to the penstock at the base of a slope. It can also be an underground powerhouse connected by a steel-lined shaft. Underground powerhouses exist in several varieties, such as the pit powerhouses preferred for high-head reaction turbines, or earth-covered

powerhouses. Both types are usually located at the base of a slope, well protected against avalanche or rockfall, within an artificial cave in rocky ground, or in a natural cave.

(2) Powerhouses close to the dam or incorporated within it are found in low-head, run-of-river power plants, where the powerhouses, together with the spillway, form part of the damming device. They are either located on the base of the dam or underground in the slopes of the valley. Incorporation of a powerhouse into a damming device is mainly used for plants on a river bay, on both river banks, and in abutment-type power plants. Powerhouses erected in the interior of the dam are mostly found in submersible power plants or in barrages, where they can be located underneath the spillway.

The superstructure of the powerhouse consists mainly of the sets, the crane, the repair shop, the erection bay, the control room, the offices, and, in underground powerhouses, very often the transformers and the high-voltage switchgear.

Powerhouses must be watertight, and must remain so throughout the useful life of the plant. Nevertheless, a certain seepage cannot be excluded, which may threaten the stability of the structure. In such cases, the seepage should be limited, for example by grout curtains, or be controlled, for example by galleries and pits equipped with pumping plants.

BIBLIOGRAPHY

1. Ann *et al. Elektrische Energietechnik (Band 4): Handbuchreihe Energie*, Heraussgeben von Th. Bohn, Rheinland: Verlag TUEV.
2. K. Bonfert *Betriebsverhalten der Synchronmaschine*, Berlin: Springer Verlag.
3. M. P. Boss A. B. B. Sécheron SA *On line monitoring*, June 5, 1997.
4. *Bulletin SEV/ASE—VSE/UCS de l'Association Suisse des Electriciens and de l'Union des Centrales Suisses d'Electricité* (1995–1997).
5. P. Henry *Turbomachines Hydrauliques*, Presses Polytechniques et Universités Romandes.
6. *Int. J. Hydropower Dams, Issues and World Atlas*, 1990 to 1997.
7. *Int. Water Power Dam Const., Issues and Handbooks*, 1990 to 1997.
8. M. A. Nicolet Hydro Power Dam, *Electrical engineering aspect of the Cleuson-Dixence project*, September 1995.
9. M. A. Nicolet Water Power Dam Constr., *Turning on the power*, June, 1998.
10. R. Noyes (ed.) *Small and Micro Hydroelectric Power Plants: Technology and Feasibility*, Park Ridge, NJ: Noyes Data Corp., 1980.
11. M. B. Petit C. G. E. E. Alsthom *Coaxial isolated-phase bus bars of high electrical current-carrying capacity, Rev. alumin., extrait n° 525*, February 1993.
12. Power Generation Committee of the IEEE Power Engineering Society, *IEEE Guide for Control of Hydroelectric Power Plants*, New York: Institute of Electrical and Electronics Engineers, 1988.
13. I. J. Raabe *Hydro Power, the Design, Use and Function of Hydromechanical, Hydraulic and Electrical Equipment*, VDI-Verlag GmbH.
14. United States Army Corps of Engineers, *Engineering and Design: Hydroelectric Power Plants Mechanical Design*, Washington, DC: Dept. of the Army, Office of the Chief of Engineers, 1980.
15. A. B. B. Sécheron SA *Les tôles magnétiques*, November 1995.
16. F. Vesligaj Aperçu quant aux choix de certains paramètres de l'alternateur-moteur de la centrale de Veytaux, *Bull. ASE n° 19*, 1967.
17. F. Vesligaj Choice of electrical characteristics for reverse (pumping-turbining) power stations, *CIGRE*, 1968.
18. F. Vesligaj L'équipement électrique de la centrale de Veytaux, *Bull. ASE—n° 16*, 1967.
19. F. Vesligaj Performance of the pumping-turbining of Capljina (Bosnia & Herzegovina), *Water Power Dam Constr.*, November 1988.

20. F. Vesligaj Problèmes rencontrés dans la réalisation des pompes-turbines de grande puissance et hautes chutes par étage et dans le démarrage de pompe. Point de vue de l'électricien A. I. M., *J. Int. d'Etude des Centr. Electr. Modern.*, 1969.

A. NICOLET
F. VESLIGAJ
Aménagement Cleuson-Dixence